Reliability Engineering and System Safety 217 (2022) 108040

Contents lists available at ScienceDirect

Reliability Engineering and System Safety

journal homepage: www.elsevier.com/locate/ress

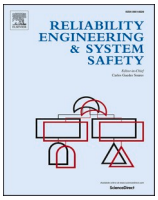

Predictive capacity of topological measures in evaluating seismic risk and resilience of electric power networks

E. Ferrario [a,b,*], A. Poulos [b], S. Castro [b], J.C. de la Llera [b,c], A. Lorca [d]

[a] School of Engineering, Pontificia Universidad Católica de Chile, Santiago, Chile
[b] Research Center for Integrated Disaster Risk Management (CIGIDEN), ANID/FONDAP/15110017, Santiago, Chile
[c] Department of Structural and Geotechnical Engineering, Pontificia Universidad Católica de Chile, Santiago, Chile
[d] Department of Electrical Engineering, Pontificia Universidad Católica de Chile, Santiago, Chile

ARTICLE INFO

Keywords:
Electric power networks
Seismic probabilistic risk assessment
Risk and resilience
Network topological measures
Component ranking
Monte Carlo simulation

ABSTRACT

Electric Power Networks (EPNs) play a fundamental role in the wellbeing of modern societies and recovery of societal functions after an earthquake. Risk and resilience analyses may identify useful network characteristics to improve EPN response and recovery during and after a severe seismic event. This work computes different functional measures in order to: (i) estimate the actual risk and resilience of EPNs; and (ii) evaluate the predictive capacity of different topological measures (TMs) relative to the EPN earthquake risk performance. The analysis is carried out on the Chilean EPN at the national, regional and substation level, by using a detailed model of the network. EPN operation was modeled using the DC optimal power flow model from the time of earthquake occurrence until full system recovery using the Seismic Probabilistic Risk Assessment framework. Seismic risk and resilience estimations of Energy Not Supplied (ENS) and number of hours with ENS have been correlated with six network TMs. Linear correlation results show that TMs provide, in general, limited insight into the criticality of the Chilean EPN. In spite of that, the strongest correlation was observed for the degree TM. Moreover, the Damage Consequence Index confirmed the rather uniformly distributed seismic risk along the country.

1. Introduction

The aim of the generation and distribution of Electric Power Networks (EPNs) is to meet the residential, commercial and industrial electric consumer demand, which may be severely affected by the disruption caused by natural hazards, in particular earthquakes [1–4]. The energy supplied by EPNs is essential in maintaining a number of critical societal functions as well as the normal operation of other lifelines [5], especially in the aftermath of an event [6,2]. Severe ground motions caused by earthquakes may damage different EPN components, compromising the ability of the system to respond and recover promptly to supply the electricity demand. Due also to the inherent interdependence within the EPN system, cascading failures have also been observed in the past due to required load redistributions that overloaded other components and led them to failure, causing severe consequences and eventual blackouts [7–9]. Interdependencies also exist between the EPN and other infrastructures and industries, affecting other apparently independent sectors [10–13], and large populations up to complete nations [6,14]. Because the unsupplied energy may range from hours till weeks before recovering the system's operation, the ability to understand, model and quantify the possible functionality loss under seismic hazard is an essential step in preventing and mitigating the undesired effects of earthquakes and finally improve resilience [15].

In general qualitative terms, resilience involves "the ability of the system to sustain or restore its basic functionality following a risk source or an event" [16]. Then, resilience refers to the complete process, i.e. the rather abrupt drop in capacity of the system as a consequence of earthquake damage of the system components, and its recovery to a new state of equilibrium between supply and demand. Such recovery process usually has different discrete stages, which are determined by the reactivation times required by the failed components. Resilience also encompasses the concept of vulnerability, which refers to an intrinsic property of the system, "the degree to which a system is able to withstand specific loads" [16], including the system's capacity to adaptation and recovery.

Several approaches, such as topological, flow, functional and logical

* Corresponding author.
E-mail address: elisa.ferrario@cigiden.cl (E. Ferrario).

https://doi.org/10.1016/j.ress.2021.108040
Received 14 March 2021; Received in revised form 1 August 2021; Accepted 3 September 2021
Available online 10 September 2021

methods, have been adopted and developed in the literature to model EPN vulnerability and resilience [8,17]. In the context of EPNs exposed to seismic hazard, extensive work has been carried out addressing several different issues. For instance, Cavalieri et al. [18] compared the performance of topological-based and flow-based models. Other authors [19], focused on the complex configuration of EPN substations and on the failure of their components that can derate the EPN performance after the earthquake. Seismic fragility functions (FFs) of EPN components are fundamental for this type of analyses, and efforts have been paid to develop accurate FFs for different components (e.g. [20,21]). Extensive literature can also be found on cascading failures that can be generated after earthquake disruptions and interdependencies between EPNs and other infrastructure networks, which is a topic of paramount importance [9,22–24]. Component criticality analyses have been carried out to identify critical components which retrofit or replacement can considerably improve the earthquake performance of the system [18,25,26], or to quantify the reduction in system performance given a failure of a component [27].

Along the same lines, the identification of the best mitigation strategies was carried out under an optimization framework to decide on the retrofit of components within a substation [28], or to maximize the load outage recovery of EPNs [29] following seismic events. Comparison between optimal robustness- and resilience-based protection strategies of EPNs against earthquakes was also carried out [30]. Differences between reliability- and resilience-driven network enhancement were highlighted elsewhere [31,32]. More recently, Venkateswaran et al. [33] proposed an optimization framework that includes both, grid-side and demand-side resilience enhancement strategies for power distribution networks exposed to earthquakes. Mitigation and restoration strategies have also been examined within a probabilistic decision support framework using Bayesian network for interconnected infrastructures affected by both seismic and tsunami hazards [34]. Recovery strategies for interdependent power and water networks were explored within a multi-objective optimization model [24]. Recovery scheduling was also addressed by using an optimization framework. Sharma et al. [35] presented a computationally efficient approach to optimize the recovery schedule of interconnected power and water networks, accounting for a multiscale recovery model, differential equations for accurate flow analyses, and new resilience metrics able to capture the temporal and spatial variations of the recovery process. Furthermore, Sharma et al. [36] proposed a new classification of interdependencies and developed a mathematical formulation to model them in the recovery of an EPN after the occurrence of a seismic event.

Another metric of resilience discussed in the literature is the EPN recovery time after the earthquake. For example, Espinoza et al. [26] quantified the recovery time of the EPN components using a probabilistic framework. Also, Bayesian networks were used for estimating the recovery time of interconnected power and water infrastructures [9] and power and telecommunication systems [12]. Furthermore, the recovery times of the EPN, transportation system, and the community were quantified by using an agent-based model within a compositional supply/demand seismic-resilience quantification framework [37].

Regarding the analysis of critical components, which is a relevant topic to prioritize components for hardening and/or recovery, planning maintenance, and improving system reliability and resilience [38], several approaches and measures have been developed in the last 60 years. Depending on the research objectives and models adopted, different measures are used to evaluate component criticality, grouped as topological measures (TMs), risk importance measures, and performance-based measures, among others [38]. Recently, two resilience-based component importance measures, i.e. optimal recovery time and resilience reduction worth, were adopted to identify critical network components of an EPN [39], and of interdependent power and water networks [40] within an optimization framework. Furthermore, Li et al. [38] presented a component importance measure based on AC power flow that accounts for cascading failures; Rocchetta and Patelli [41] analyzed the effects of uncertainty on the quantification of different vulnerability metrics of EPNs by using flow-based and topological models. Sherb et al. [42] developed a procedure to assess component importance of EPNs exposed to wind hazards, accounting for both, common cause failures and cascading failures, and using Birnbaum's measure, criticality importance, and an additional measure based on load losses. In the context of seismic hazard, a vulnerability metric that combined the component probability of failure and the component importance measured in terms of the drop in system performance was adopted earlier [18,25] and applied to the IEEE 118 Bus Test Case. Liu et al. [43] used two importance measures, i.e. risk achievement worth and risk reduction worth, to identify critical substation components that need to be prioritized for seismic retrofit, and obtained numerical results for the modified CIGRE medium voltage test network. In Espinoza et al. [26], a component criticality analysis based on the Fussell–Vesely importance measure was carried out on the partially integrated EPN system in the north of Chile to identify components that, if invulnerable, would contribute more to the reduction of losses at the system level.

Some of the above mentioned works (e.g. [39]), compared the adopted importance measures with TMs, and provided a ranking of component importance, identifying those whose failures can induce significant structural damage to the network [44,45]. It is still an open discussion whether TMs may fully capture the vulnerabilities of EPNs [46,41]. However, it has been shown that selective node removals based on a topological ranking, such as decreasing degree order, produce a stronger impact on system vulnerability [44,47,48]. Also, Fang and Zio [49] performed hierarchical clustering on the Italian EPN and found that most of the nodes identified as important through clustering coincided with those with the highest centrality values, except for a few exceptions. Conversely, Rosato et al. [50] focused on the system functional vulnerability and showed that only a small number of components with high relevance from a functional viewpoint (flow) can be detected through topological centrality measures, which are in turn associated with the structural vulnerability of the system. Also, LaRocca et al., [51] compared topological-based and flow-based models to understand the tradeoff between simplicity and accuracy of these models and found that the choice of the best EPN model depends on the objective of the analysis. Furthermore, Rocchetta and Patelli [41] found that the capacity of TMs for contingency ranking was questionable, but they highlighted the positive features of topological models and proposed further comparisons.

However all this bulk of knowledge, little attention has been paid so far to the predictive capacity of TMs in terms of earthquake risk performance of EPNs. Buriticá-Cortés et al. [25] adopted three TMs, nodal degree, betweenness and traffic, in order to rank component criticality. Critical components were retrofitted and the EPN performance reanalyzed under several earthquake scenarios. Results were then compared with a much more elaborate vulnerability metric [18,25] that is able to identify a set of critical components that once retrofitted considerably improve the system's performance. While these results can be very useful in practice for an existing network, they may not be easily used in a preliminary assessment. Indeed, the vulnerability measure proposed requires simulation of a large number of scenarios to account for the ground motion uncertainty, and hence it cannot provide a-priori good blind estimations. Also, the criticality analysis carried out by Espinoza et al. [26] presents the same limitation, and though it is comprehensive, it is computationally prohibitive for large systems because it requires simulating all earthquake scenarios as many times as the number of EPN components, selecting each time a different component as invulnerable.

Given this context, the objective of this research is twofold. First, to obtain the best possible estimation of seismic risk and resilience of the Chilean integrated EPN exposed to earthquake hazard using a Seismic Probabilistic Risk Assessment (SPRA) framework, which is a comprehensive framework that accounts for the uncertainties in the recurrence model, epicenter, and magnitude of the earthquake event, as well as the fragilities of the system [52,53,26]. The model developed considers 994

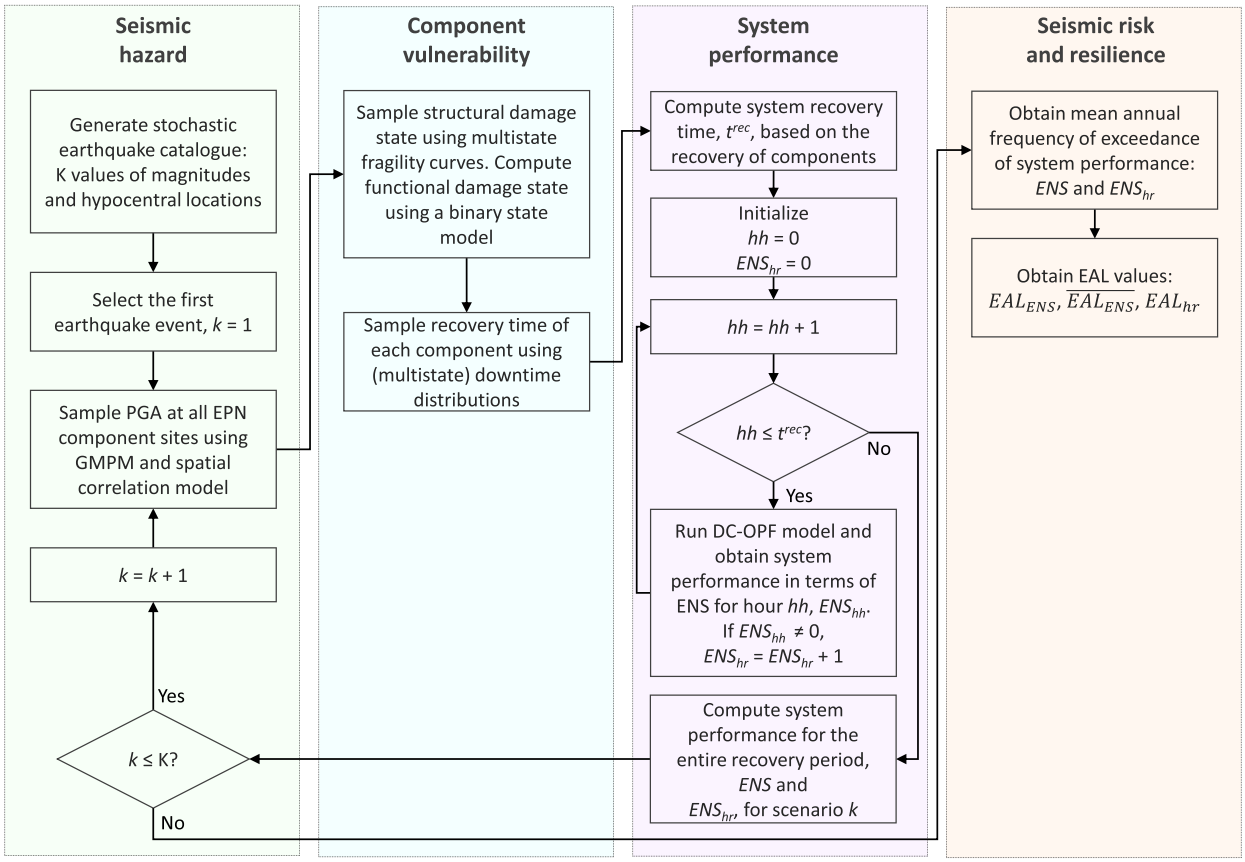

Fig. 1. Illustrative diagram of the SPRA framework adopted in this work.

substation nodes, while the one used for the Electric Coordinator in the country has 280 nodes. Therefore, risk and resilience analyses are carried out at the national, regional, and component levels and for each level, the EPN performance is determined in terms of the Energy Not Supplied (ENS) and the number of hours with ENS after the occurrence of a severe earthquake by using the DC—OPF model until full system recovery (resilience index). The second research objective is to evaluate the predictive capacity of classical and extended TMs of seismic risk of EPNs. The aim of this part of the research is to verify the level of correlation that risk results –at a component level– present with some of the classical TMs of the network, such as degree, betweenness centrality, closeness centrality, minimum distance to a source, entropy degree, and electrical betweenness. The Damage Consequence Index (DCI) is also computed from the simulation results as a proxy of the component criticality for a post-disaster assessment [54]. The analyses were carried out on the 994 node integrated Chilean EPN and the most recent seismic hazard model for the country [55].

This work introduces improvements to the work done previously in the Chilean EPN [26]. First, it focuses on the complete interconnected Chilean EPN system, not only the north segment as done earlier [26]. It also includes a validation of the integrated EPN model in normal operation conditions, which implies that the dispatch of energy resembles that of the one used in the country. Third, it carries out seismic risk and resilience analyses at different geographical scales. And fourth, it provides more detailed insights on the correlation between risk and resilience results and topological properties of the EPN. Herein, the recovery time is estimated using a probabilistic approach without entering into the details of the recovery process as previously done under an optimization framework [35,36]. The contribution of this work lies primarily on: (i) the high-resolution model of the integrated Chilean EPN used in conjunction with the SPRA framework; (ii) the detailed study of different TMs as predictors of risk and resilience results using a detailed network model; (iii) the potential identification of critical EPN components or clusters to use in a preliminary assessment to improve EPN earthquake resilience; and (iv) the implications on risk and resilience of the longitudinal EPN structure (topology), which runs from north to south along the country, and coincides with the typical rupture direction of the controlling subduction seismic source.

Section 2 of this article shortly introduces the SPRA framework of EPNs and provides risk and resilience results for the 994 node Chilean EPN (first objective); Section 3 presents the TMs of the Chilean EPN and illustrates the results obtained in terms of the existing correlations with risk results (second objective); and, Section 4 presents the conclusions of this work. Finally, the notation used in the DC—OPF model, the data collection process, and the model validation of the Chilean EPN are illustrated in Appendices A, B, and C, respectively.

2. Network modeling and probabilistic seismic risk and resilience assessment of EPNs

This Section summarizes the methodology used in modeling an EPN and its earthquake risk quantification. Although the concepts applied herein are completely generic, results will be applied to the case of the integrated Chilean EPN system, which has distinctive features from other EPNs in seismic environments elsewhere in the world. In particular, the longitudinal structure of the Chilean network coincides with the main seismic source that controls earthquake risk in the country, which runs north to south at the convergence of the continental plate riding on top of the pacific plate (subduction) at very high convergence rates ~ 68 mm/year [56]. Moreover, the narrow width of the country implies another important feature of the seismic intensity measures used in computing risk for the EPN, which is quite uncommon for seismic settings elsewhere. Consequently, the seismic risk of the Chilean EPN presents features that are significantly different from similar networks in

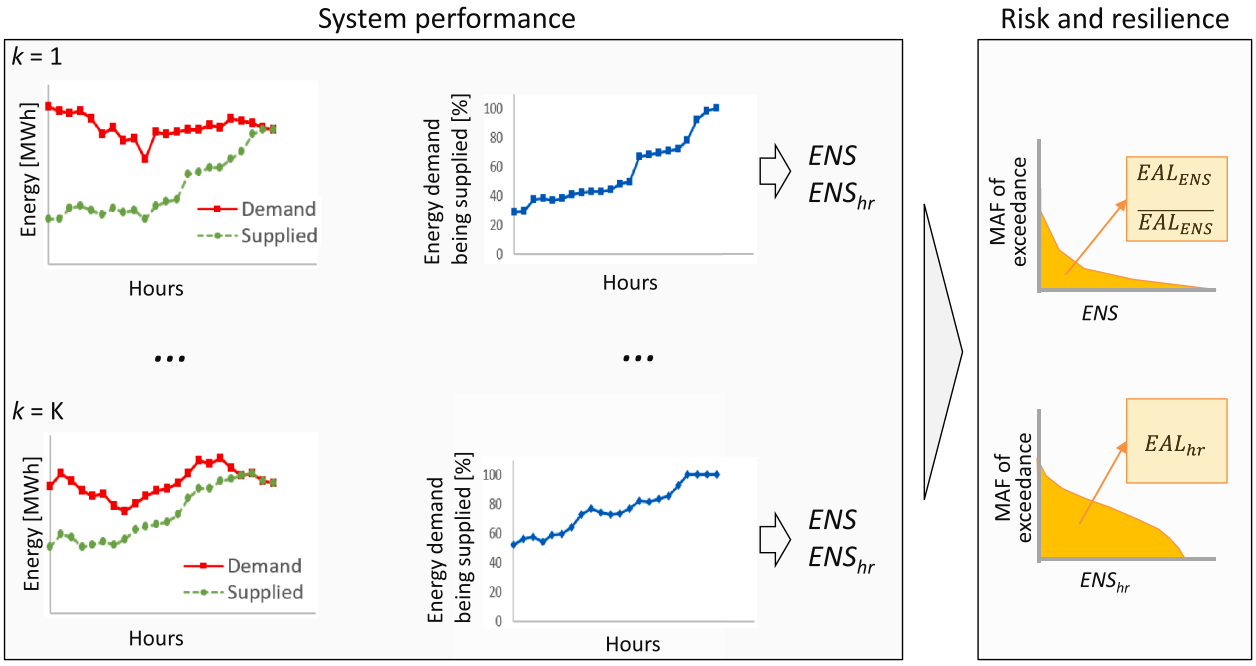

Fig. 2. Left box: Schematic illustration of the typical results obtained for each SPRA realization; Right box: expected annual losses corresponding to all realizations.

other seismic environments.

2.1. SPRA framework

The assessment framework of seismic risk and resilience for EPNs is presented in Fig. 1 and is based on Monte Carlo simulation, and is similar to that used in previous works (e.g. [52,53]). The main steps of the procedure are to: (i) perform a seismic hazard analysis aimed to the generation of a stochastic catalog of earthquake scenarios in the region under analysis and sampling of ground-motion intensities at the EPN component locations; (ii) assign component vulnerabilities by estimating component damage states, functionality, and recovery time; (iii) evaluate the EPN system performance throughout the restoration process until service is fully restored; and (iv) compute seismic risk and resilience using the response of the system to all simulated scenarios.

The procedure starts by constructing a synthetic earthquake catalog using a recurrence model of seismic events proposed earlier [55]. Peak ground accelerations (PGAs) at the location of each component of the EPN are sampled using the ground motion prediction model (GMPM) developed by Abrahamson et al. [57] and the spatial correlation model developed by Goda and Atkinson [58]. Using these Intensity Measures (IMs), the next step is to estimate earthquake damage for each scenario at the EPN component level and the time needed to recover each component. Fragility functions and downtime distributions are taken from previous work [59], and consider a multistate model with four damage states for anchored components. Damage states for substations and power generation units, which are the main components at risk in EPNs, are randomly sampled as well as their corresponding recovery times. Regarding component functionality, it is assumed conservatively a binary status, where the operation of a component stops if it has any level of structural damage (i.e. minor or greater).

With all downtimes estimated for a given realization, the operation of the EPN is simulated over time based on component functionality. This implies solving the DC—OPF model presented next every hour throughout recovery of all EPN components. As a result of this analysis, the hourly ENS is estimated for the realization. Two measures of system performance (losses) were evaluated: (i) the total unsupplied energy due to earthquake damage (ENS); and (ii) the number of hours with energy-not-supplied (ENS_{hr}), which accounts for the duration of operation interruption due to damage on the EPN, which is a proxy of the recovery time for system functionality. EPN losses do not occur at consecutive times, since given a damaged configuration, energy supply also depends on the energy demand and the available power generation capacity from renewable sources, which vary in time. ENS_{hr} is a good estimate of the effective time without service and is used hereafter as a measure of system resilience.

Seismic risk of the EPN is characterized by a mean annual frequency (MAF) of exceedance, $\lambda_{SP}(sp)$, of a threshold value, sp, of the system performance variable SP. By using total probability, seismic risk of a spatially distributed system of n components can be stated as [53]:

$$\lambda_{SP}(sp) = \nu \int_{\Omega \subseteq \mathbb{R}^n} \mathrm{P}(SP > sp | \boldsymbol{IM} = \boldsymbol{im}) f_{IM}(\boldsymbol{im}) d\boldsymbol{im} \quad (1)$$

where ν is the mean annual rate of significant earthquake events (those of "engineering interest"); $\mathrm{P}(SP > sp|\boldsymbol{IM} = \boldsymbol{im})$ is the conditional probability that SP exceeds the threshold value, sp, given an intensity measure of ground motion, $\boldsymbol{IM} = \boldsymbol{im}$, with $\boldsymbol{IM}$ a vector of n random variables representing the ground-motion IMs, such as PGAs, at all n sites of network components; $f_{IM}(\boldsymbol{im})$ is the joint probability density function of the ground motion IMs; and the integral is over the domain $\Omega \subseteq \mathbb{R}^n$, of the studied intensities and adds all possible cases. Monte Carlo is used here to approximate the complex integral solution of Eq. (1) and the MAFs of exceedance of the two considered performance measures, ENS and ENS_{hr}, which are computed using the response of the EPN to all simulated earthquake realizations. Also note that the area below the MAF curve represents the Expected Annual Loss (EAL). In this work, three EALs are computed: (i) EAL_{ENS}; (ii) EAL_{hr}, and (iii) $\overline{EAL_{ENS}}$, which is the ENS normalized by the annual energy demand.

A schematic graphical representation of these calculations is presented in Fig. 2. The first column plots in the box of the left show the hourly supplied energy from the time of the earthquake event until full system recovery for the *k-th* realization. The second column plots in the left box present the percentage of energy demand being supplied over time. These are typical resilience curves that show the quick drop of system functionality after the event and its restoration over time. Note that this curve is not monotonically increasing due to the variability in the energy demand and the renewable power generation capacity. The

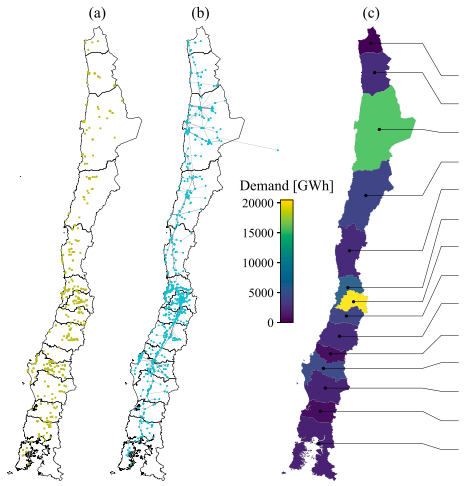

Country Region	Compo-nents [#]	Generation units [#]	Sub-stations[#]	Power gen capacity [MW]	Yearly energy demand [GWh]
Arica-Parinacota (AP)	22	6	16	32	83
Tarapacá (TP)	58	23	35	289	2651
Antofagasta (ANTOF)	212	55	157	5775	14970
Atacama (ATCMA)	121	44	77	2253	4218
Coquimbo (COQ)	85	36	49	1058	2477
Valparaíso (VALPO)	165	55	110	3095	6596
Metropolitan (RM)	223	42	181	981	20492
O'Higgins (LGBO)	102	29	73	1327	4300
Maule (MAULE)	100	37	63	1791	2593
Ñuble (NUBLE)	31	8	23	48	838
Biobío (BBIO)	192	82	110	4313	4663
Araucanía (ARAUC)	60	21	39	137	2035
Los Ríos (RIOS)	44	25	19	292	696
Los Lagos (LAGOS)	79	37	42	502	1908
Total	1494	500	994	21900	68526

Fig. 3. Schematic view of the EPN with (a) power plants; (b) substations and transmission lines; and (c) Chilean regions interconnected by the electric system and data associated with the regional network characteristics.

ENS and ENS_{hr} values obtained for each realization are used to build the exceedance MAF by Monte Carlo simulation. These curves represent the risk and the associated enclosed areas the expected annual losses, which are a measure of the resilience of the system.

To minimize the computational work involved in the SPRA, importance sampling was used for earthquake magnitudes in order to increase the sampling rate of higher magnitude earthquakes as proposed earlier (e.g. [52,53]). For further details on the procedure adopted in this work, the interested reader is referred to the literature [53,60].

2.2. EPN modeling

This research uses an optimal power flow (OPF) approach that is able to dispatch electricity into the EPN to meet the energy demand by improving the overall system performance, i.e. by minimizing operating costs, and ensuring that the system constraints are not violated [61]. Specifically, the DC—OPF model is adopted here given its simplicity and ability to always provide a solution. Indeed, it is a linear approximation of the more complex AC—OPF model. The DC—OPF model consists of a linear relationship between power flow through the lines and power injection at the generation nodes, and is typically adopted in practice for transmission networks [62,63], which are characterized by a very low resistance value and by voltages similar to the nominal values. It allows the calculation of the amount of energy generated by each power generation unit, the amount of (un)supplied energy to substations, the power flowing through the lines, and the voltage angles at steady state for a specific scenario.

The DC—OPF problem aims to minimize the total costs of energy generation and unsupplied energy, as illustrated in the objective function of Eq. (2) for a specific hour of interest (e.g. [26]) and subjected to the constraints described in Eqs. (3)–(9). The notation used in the formulation of the problem is given in Appendix A, Table A.1. The DC—OPF problem may be stated as:

$$\min\left\{\sum_{g\ \epsilon\ \mathscr{G}} P_g \cdot c_g^{gen} + \sum_{n\ \epsilon\ \mathscr{N}} LS_n \cdot c_n^{LS}\right\} \tag{2}$$

s.t.

$$\sum_{g\ \epsilon\ \mathscr{G}(n)} P_g + \tau^{loss}(LS_n - D_n) + \sum_{l\ \epsilon\ \mathscr{L}(n)} f_{l,n}^{in} - \sum_{l\ \epsilon\ \mathscr{L}(n)} f_{l,n}^{out} = 0,\ \forall\ n\ \epsilon\ \mathscr{N} \tag{3}$$

$$0 \le P_g \le P_g^{max} \cdot u_g^{op},\ \forall\ g\ \epsilon\ \mathscr{G}^T,\ \mathscr{G}^T \subset \mathscr{G} \tag{4}$$

$$0 \le P_g \le P_g^{hist} \cdot u_g^{op},\ \forall\ g\ \epsilon \mathscr{G}^R,\ \mathscr{G}^R \subset \mathscr{G} \tag{5}$$

$$0 \le LS_n \le D_n,\ \forall\ n\ \epsilon\ \mathscr{N} \tag{6}$$

$$f_l = \frac{S_0}{x_l}(\theta_n - \theta_h) \cdot u_l^{op},\ \forall\ l\ \epsilon\ \mathscr{L}, n, h\ \epsilon\ \mathscr{N}(l) \tag{7}$$

$$-f_l^{max} \le f_l \le f_l^{max},\ \forall\ l\ \epsilon\ \mathscr{L} \tag{8}$$

$$\theta_{n_{ref}^{isl}} = 0,\ n_{ref}^{isl}\ \epsilon\ \mathscr{N},\ isl = 1,\ \ldots,\ N_{island} \tag{9}$$

Eq. (3) represents the power balance at node n and considers four terms: the total power generated by the power generation units connected to the node; the second term represents the power consumption in the node, where τ^{loss} is the power loss factor, which is assumed to be constant and equal to 1.078, i.e. an increase of 7.8% in energy consumption to account for power losses; and the last two terms represent the difference between incoming and outgoing power flows. Eqs. (4) and (5) are constraints related to the maximum power generation capacity of unit g, which differs by generation unit and accounts for uncertainties in power generation from renewable power units. If g belongs to the set of thermal power plants, $\mathscr{G}^T$, the maximum power generation capacity is equal to the nominal value, P_g^{max}, and constant over time; instead, if g belongs to the set of renewable power plants, $\mathscr{G}^R$, the maximum power generation capacity is assumed equal to the historical value of power generation, P_g^{hist}, which varies with the hour considered. The minimum power generation capacity was set to 0 and a ramp capability was not considered. The constraint in Eq. (6) establishes that the unsupplied power in a node cannot be higher than the energy demand of that node. Furthermore, Eq. (7) represents the flow through line l; and given the DC approximation, the magnitude of the voltage in all the nodes is fixed to 1 per unit (p.u.), so the flow through line l depends only on the voltage angle differences. Also, Eq. (8) limits the flow through line l to its maximum capacity, and Eq. (9) sets the voltage angle to zero of the reference node(s). If the network is fully connected, $isl = 1$, and one reference node is identified; otherwise, if islands are generated, N_{island} reference nodes should be identified and their voltage angles set to zero.

Notice that the service interruption cost, c_n^{LS}, in Eq. (2) is assumed equal for all substations $n \in \mathscr{N}$, neglecting possible load priorities, and is fixed to a very large value to penalize the occurrence of load shedding in the optimization problem. A binary state is considered for the functionality of substations and power generation units, where the value 0 means that the facilities stop working due to structural damage and 1

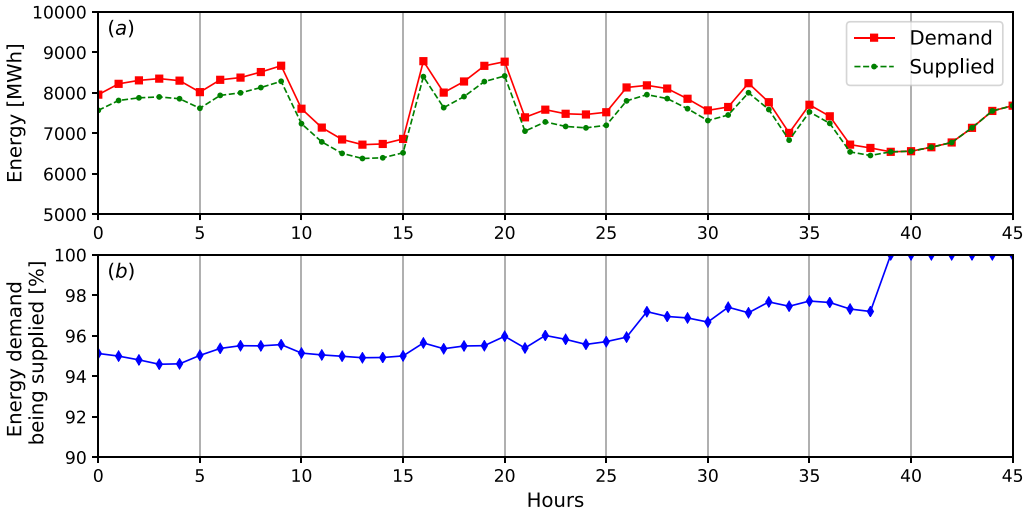

Fig. 4. Typical system performance over time for the k-th realization ($k = 11{,}237$): (a) energy demanded and supplied; and (b) percentage of the energy demanded being supplied.

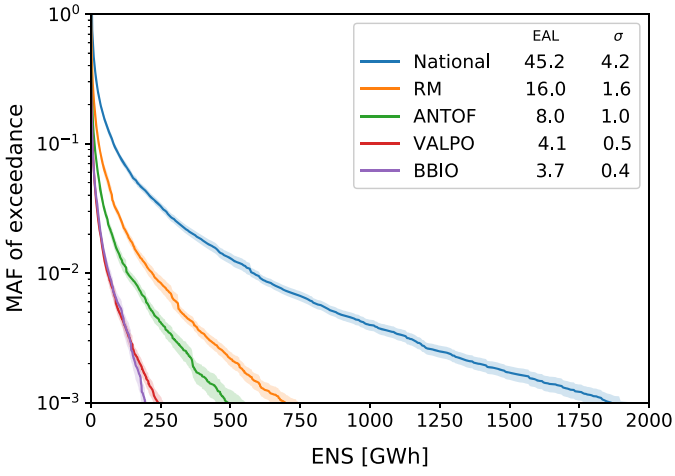

Fig. 5. MAFs of exceedance of ENS (solid lines) and 95% confidence intervals (light color shaded areas). EAL_{ENS} values and standard deviations are given in the legend.

that are operative. The functionality of transmission lines is derived from the functionality of substations. Thus, transmission lines are considered in operation, if and only if they connect two substations in operation. For a reference year, the information on energy demand and energy generation from renewable sources is retrieved from historical data by considering historical hourly energy demand (load) profiles and historical hourly energy generation profiles from renewable sources. The use of historical energy demand and generation profiles leads better results to reflect real operation, rather than using values derived from an uncertain cost of water or energy demand.

2.3. Seismic risk of the Chilean EPN

The Chilean national electrical system (SEN) covers most of the national territory and serves 98.5% of the Chilean population [64]. To build the Chilean EPN model, both topological and electrical data related to power generation units, substations, transmission lines and loads were retrieved from different official Chilean databases [65–67]. The reference year was 2017, and Fig. 3 illustrates: (a) power generation units; and (b) substations and transmission lines of the SEN. Shown in the figure are the 14 out of 16 Chilean regions electrified by the SEN with the relevant regional features, total installed power generation capacity, annual energy demand (energy withdrawal), and number of all components, generation units and substations. One substation is located in Argentine (Central Salta, Fig. 3(b)) and is assigned to the Antofagasta region since it is connected to a substation in this region. Appendix B presents more information on the data collection process and the associated limitations of the data.

The model was validated by running the DC—OPF model every hour for a time window of one year in normal operation condition. The conditions imposed on to the model were: (i) to satisfy the supply of historical energy demand; and (ii) to approximately reproduce the normal operation of the actual system. Results of the model validation are presented in Appendix C.

2.3.1. Results at country level

The Chilean EPN model has been exposed to the occurrence of 50 thousand stochastic realizations of earthquake events consistent with the Chilean seismic hazard [55]. An earthquake event can randomly occur within a year, in any of the 8760 hours of that year. Before the occurrence of the earthquake, the EPN system is assumed to be fully operative. In addition, component recovery is carried out simultaneously on all components assuming unlimited resources of repairing teams and materials, as well as equal priority for the restoration. The recovery time of the entire system is controlled by the component with the largest recovery time. It is also assumed that undamaged power generation units are available for generation at any time. To account for cases in which recovery could not be completed within a year, an additional complete year was considered. Such cases tend to occur if the earthquake happens at the end of the year; the additional year is identical to the reference year.

Fig. 4 presents a typical example of the energy supplied (Fig. 4a) and percentage of energy demand satisfied (Fig. 4b) as a function of time after the earthquake. In this case, the total ENS is equal to 12,440 MWh and the hours with ENS are 39. Notice that the rapid recovery from hour 38 to hour 39 in Fig. 4(b) is due to the recovery of a load substation that allows supplying its associated energy demand. In addition, in this example, the total time needed to recover all damaged components is 108 h, but the EPN system is able to fully supply the energy demand from hour 39.

Shown in Fig. 5 are the MAFs of exceedance for ENS (solid lines), bounded by the 95% confidence intervals (colored shadows); EAL_{ENS} values and associated standard deviations are also reported for each case. Results are reported at country level and for the four regions with

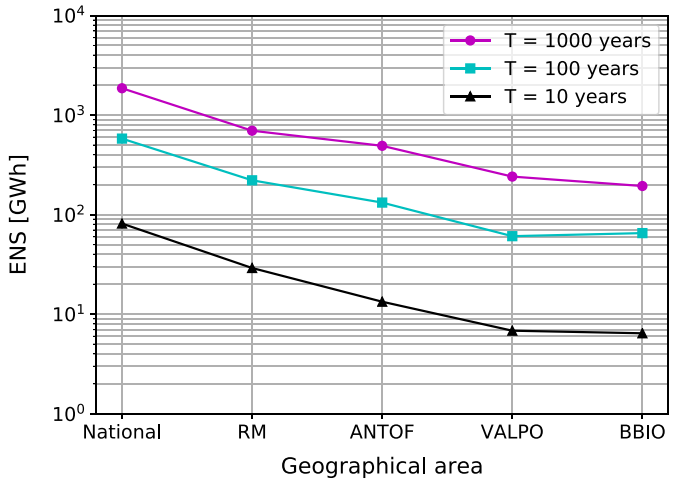

Fig. 6. ENS corresponding to return periods of 10, 100, and 1000 years for the top 4 ranked regions in descending order and the whole country ("National").

the highest annual energy demand. Because there is a strong positive Pearson correlation coefficient of 0.98, between regional energy demand and EAL_{ENS}, the chosen regions also have the highest EAL_{ENS}. Country level EAL_{ENS} is equal to 45.18 GWh, and considering that the average hourly energy demand in Chile is about 7.82 GWh, this EAL_{ENS} represents 6 h of total blackout per year in the country. The Metropolitan Region (RM) is the most critical with $EAL_{ENS} = 16.02$ GWh, followed by Antofagasta with 7.98 GWh. The Valparaíso and Biobío regions are similar in terms of average losses with $EAL_{ENS} = 4$ GWh. Since the mean hourly energy demand in the RM is about 2.34 GWh, the EAL_{ENS} is equal to almost 7 h of total blackout per year.

Return periods are the inverse of the MAF, so a MAF of exceeding $ENS = 10$ GWh at country level is 0.51, corresponding to a return period of about two years. For larger return periods of 10, 100 and 1000 years, the country's ENS will be 81.54 GWh, 581.31 GWh and 1862.36 GWh, respectively (Fig. 5). Please note that the values associated with a constant MAF of exceedance, say 10^{-3}, correspond to the uniform regional risk of ENS corresponding to a return period of 1000 years. Thus, Fig. 6 shows the ENS corresponding to uniform risk with return periods of 10, 100, and 1000 years for the country and the top 4 regions in ENS descending order.

The EAL_{ENS} ranking for the Chilean regions is presented in the left plot of the colored map of Fig. 7. The central plot shows the regions ranked based on normalized EAL, $\overline{EAL_{ENS}}$. It is apparent that the normalization changes the criticality of regions, making Arica-Parinacota, which is the one with lowest annual energy demand, 83.95 GWh (denominator), the most critical one. Indeed, this region is the least critical in EAL_{ENS} with 71 MWh. Other $\overline{EAL_{ENS}}$ critical regions in decreasing order are Biobío, Araucanía, Metropolitan, Atacama, and Ñuble.

At country level, $EAL_{hr} = 395\ h$ ($\sim$ 16.5 days) with ENS; recall that this measure of time is not related to the level of service lost. At regional level, the four regions reported in Fig. 5 also lead to the highest EAL_{hr} with unsupplied energy, which value is larger than 100 h with the highest number of units failed on average. The correlation between the regional energy demand and EAL_{hr} is 0.83, and the correlation between the average number of failed components in a region and the regional EAL_{hr} is 0.93. Downtime of substations and power generation units are assumed to be independent of the voltage level or unit size, and the geographical area. The complete EAL_{hr} ranking is shown in the right plot of Fig. 7. On average, the region with the shortest time window with unsupplied energy of 10 h is Arica-Parinacota; this region is also the one with the smallest number of installed units, 16 in total.

Similarly, shown in Fig. 8 are the MAFs of exceedance (solid lines) of hours with unsupplied energy (ENS) at country level and for the four regions with the highest annual energy demand. The 95% confidence intervals are also presented as colored shadows. The EAL_{hr} values and their standard deviations are also reported in the box of the Figure. At the country level, the MAF of exceedance of 168 h (one week) is equal to 0.43, which corresponds to a return period of 2.3 years. Fig. 9 shows the ENS_{hr} associated with a uniform risk with return periods of 10, 100, and 1000 years for the top 4 regions (ranked in descending order), as well as for the whole country.

The results reported at national level in these analyses are in the same order of magnitude as the impacts registered after the Mw8.8,

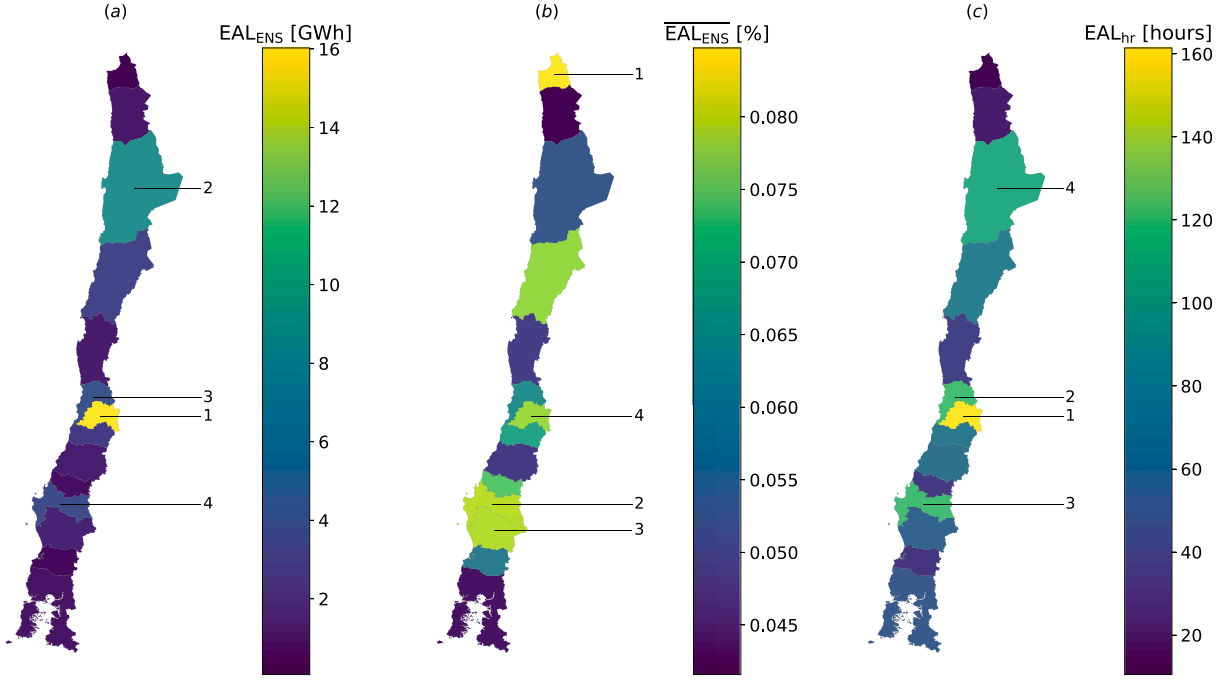

Fig. 7. Regional EAL values: (a) EAL_{ENS}; (b) $\overline{EAL_{ENS}}$; and (c) EAL_{hr}. Ranking order of the first four most critical regions is also reported.

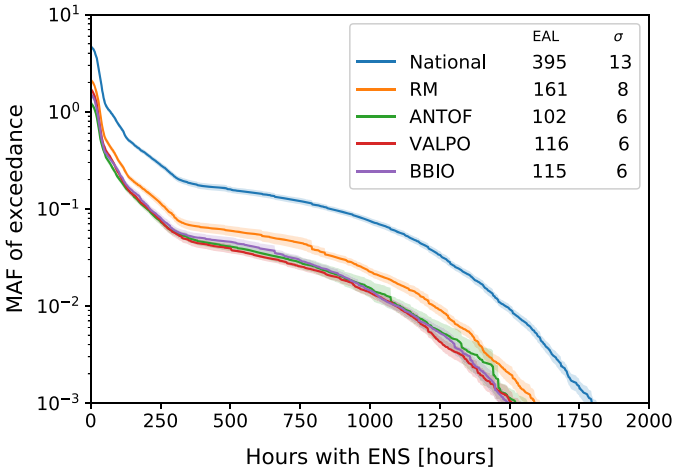

Fig. 8. MAFs of exceedance of a given value of hours with ENS (solid lines) and 95% confidence intervals (light color shaded areas). EAL_{hr} values and standard deviations are given in the legend.

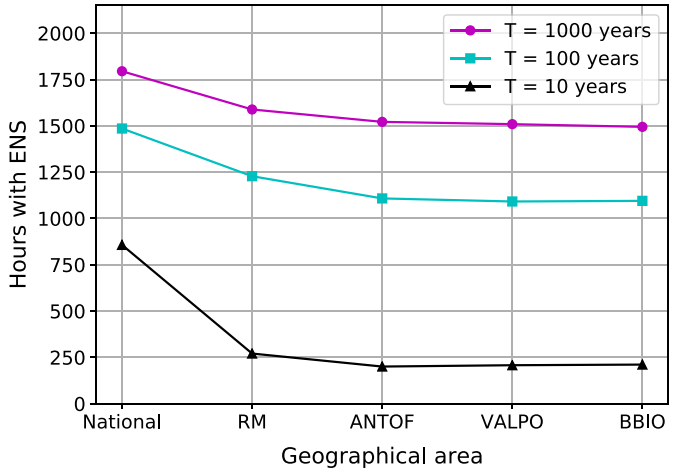

Fig. 9. Hours with ENS corresponding to return periods of 10, 100, and 1000 years for the top 4 ranked regions in descending order and the whole country ("National").

2010 Maule earthquake in Chile, which resulted in an immediate blackout of 4522 MW [6,68]. Differences result from two main factors, the electricity demand was lower in 2010 than in 2017, and the affected EPN at the time, the Chilean Central Interconnected System, was smaller than the SEN.

2.3.2. Results at component level

Correlation plots between the three EAL measures and the energy demand for each load substation are presented in Fig. 10; Pearson correlation coefficients, R, are also reported in each plot. The highest positive correlations happen between energy demand and EAL_{ENS} (plot (1, 3)), and between the $\overline{EAL_{ENS}}$ and the EAL_{hr} (plot (2, 1)). The higher the energy demand of a load substation, the higher the EAL_{ENS} (plot (1, 3)). It should also be expected that the higher the EAL_{hr} of a load substation, the higher the $\overline{EAL_{ENS}}$ (plot (2, 1)). Such is the case because the larger the recovery time of a load substation, the larger the percentage of unsupplied energy relative to the total energy demand. Please notice that this effect is not apparent between EAL_{hr} and EAL_{ENS} (plot (1, 2)), since the total ENS may be small in magnitude, but still important relative to the energy demand. These results are different from those at regional level, where we observe high positive correlation between EAL_{ENS} and EAL_{hr}. This is because EAL_{hr} at regional level depends on the combination of available components and not simply the sum of the unavailable hours of each component. All other scatter plots reflect no significant linear correlations among response quantities of the EPN, which implies that they provide different information and network characterizations in statistical terms.

3. Analysis of topological measures

In this Section, the risk obtained above may be correlated with different TMs of the network to investigate if some characteristics of the structure of the network may have some predictive capacity in terms of estimating seismic risk, at least qualitatively. Section 3.1 briefly introduces the TMs adopted herein; and Sections 3.2 and 3.3 present the results.

3.1. Topological measures used

Three classical network TMs, degree [69,70], betweenness [70], and closeness [70,71] are initially considered. We also include the minimum shortest path from any load substation to any generation unit, as well as two extended TMs, namely the entropy degree and the electrical betweenness, which are intended to capture electrical features of the network [72,73]. Except for the minimum distance to a generation unit and the closeness centrality that refer only to load substations n with $n \in \mathcal{N}^D$, where $\mathcal{N}^D$ is the set of substations with energy demand, the other TMs are computed for all n substations. A brief explanation of these measures is provided next, and readers are referred to previous references and to [74,8] for further details.

In short, the degree of substation n (node) represents the connectivity of the node with its neighbors, and is defined by the number of neighboring nodes; a node with many connections is a hub in the network. The betweenness centrality of substation n represents the number of shortest paths that pass through node n, considering the shortest paths between all pairs of nodes, excluding node n. Shortest paths are here computed considering an undirected graph, which does not differentiate between generation and load nodes. The minimum distance of load node n, $n \in \mathcal{N}^D$, to a source node m, $m \in \mathcal{N}^G$, where $\mathcal{N}^G$ is the set of substations with power generation, refers to the shortest path distance from load node n to any generation substation m. The shortest path distance is here computed considering the length of each line, and it is given in km. Furthermore, closeness centrality of load node n represents how close is the node from the rest of the generation nodes m, $m \in \mathcal{N}^G$, and is defined as $C_C(n)$ and the expression [74,75]:

$$C_C(n) = \frac{N_G - 1}{\sum_{m \in \mathcal{N}^G} d_{min}(n, m)} \tag{10}$$

where N_G is the total number of substations in $\mathcal{N}^G$ and $d_{min}(n, m)$ is the shortest path distance in km between load node n and generation node m. Entropy degree of substation n extends the concept of degree by considering not only the number of links connected to the node, but also the weights of the links and their distribution among links [73]. The entropy degree of substation n, $C_D^{ext}(n)$, is [72,73]:

$$C_D^{ext}(n) = \left(1 - \sum_{h \in \mathcal{N}} \bar{f}_{l_{nh}} \cdot \log\left(\bar{f}_{l_{nh}}\right)\right) \sum_{h \in \mathcal{N}} f_{l_{nh}}^{max} \tag{11}$$

where $f_{l_{nh}}^{max}$ is the maximum power flow in the line connecting substations n and h; and $\bar{f}_{l_{nh}}$ is the power flow limit of line_{nh} normalized relative to the sum of the power flow limits of all lines connected to n.

Electrical betweenness of substation n represents the total transmission power taken by node n within the power grid. It extends the concept of betweenness centrality by considering: (i) specific functions of generation, transmission, and load nodes; (ii) the contribution of each transmission line when power is transmitted from generation nodes to

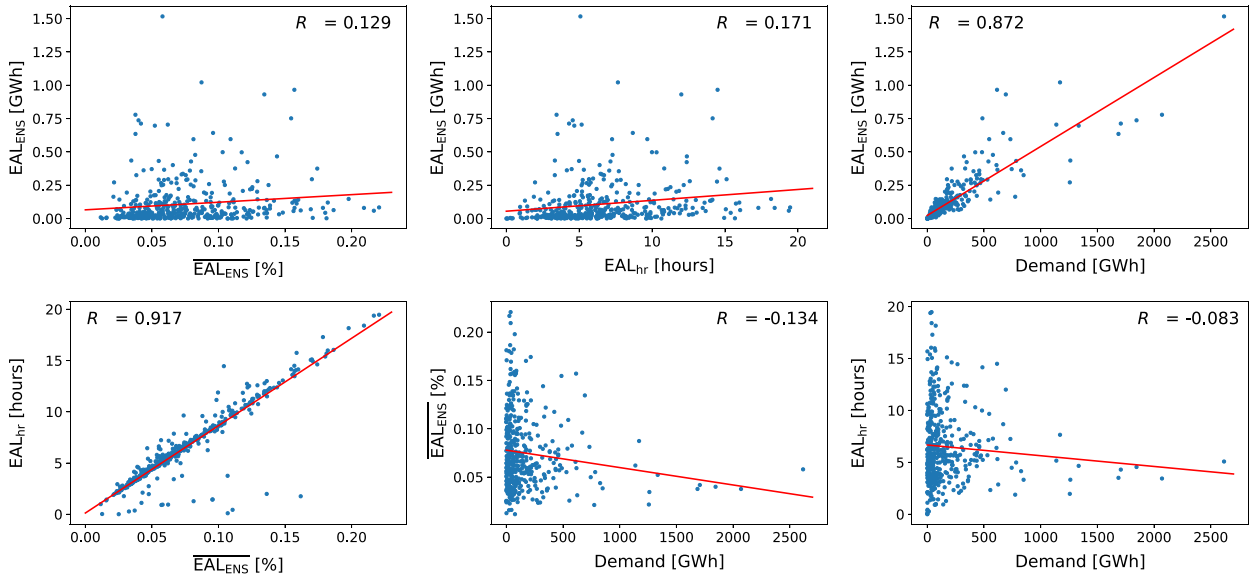

Fig. 10. Correlation analyses between energy demand of load substations and EAL values represented by EAL_{ENS}, $\overline{EAL_{ENS}}$, and EAL_{hr}. Linear regression and Pearson correlation coefficients, R, are also reported.

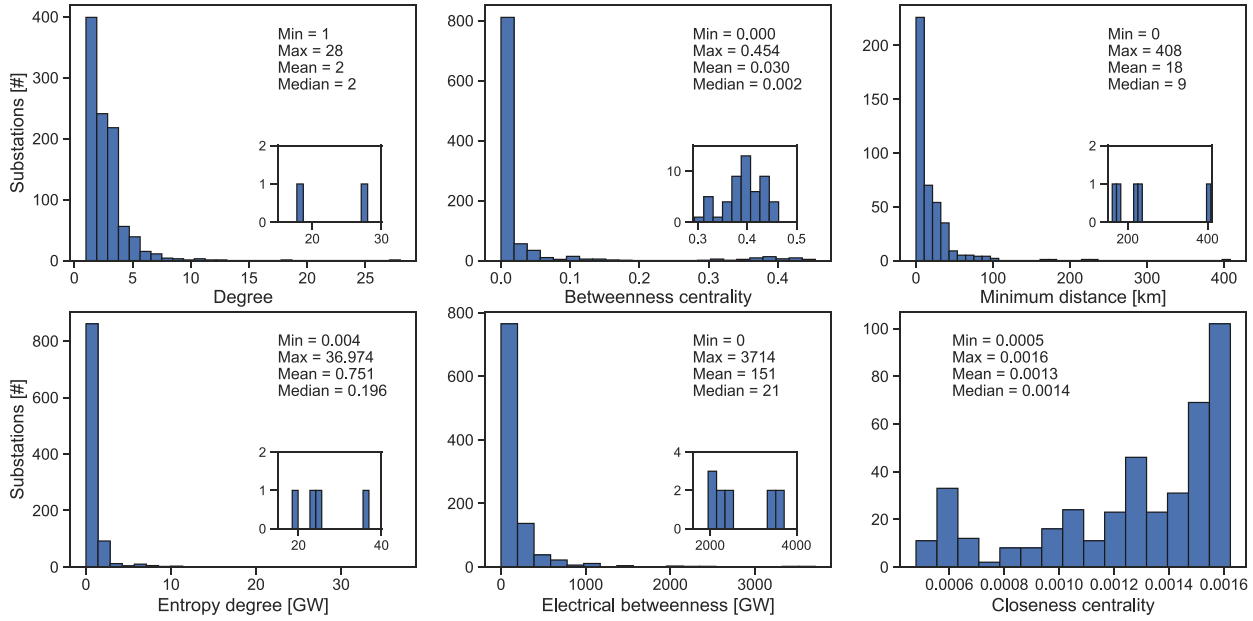

Fig. 11. Histograms of the TMs analyzed with minimum, maximum, mean and median values.

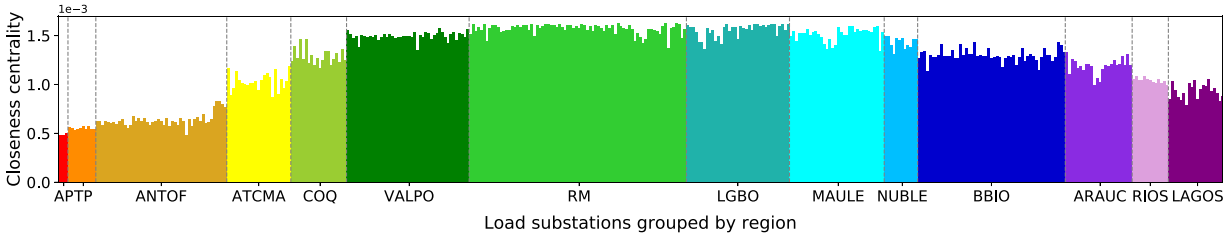

Fig. 12. Closeness centrality for load substations; colors represent different regions ordered southward from left to right.

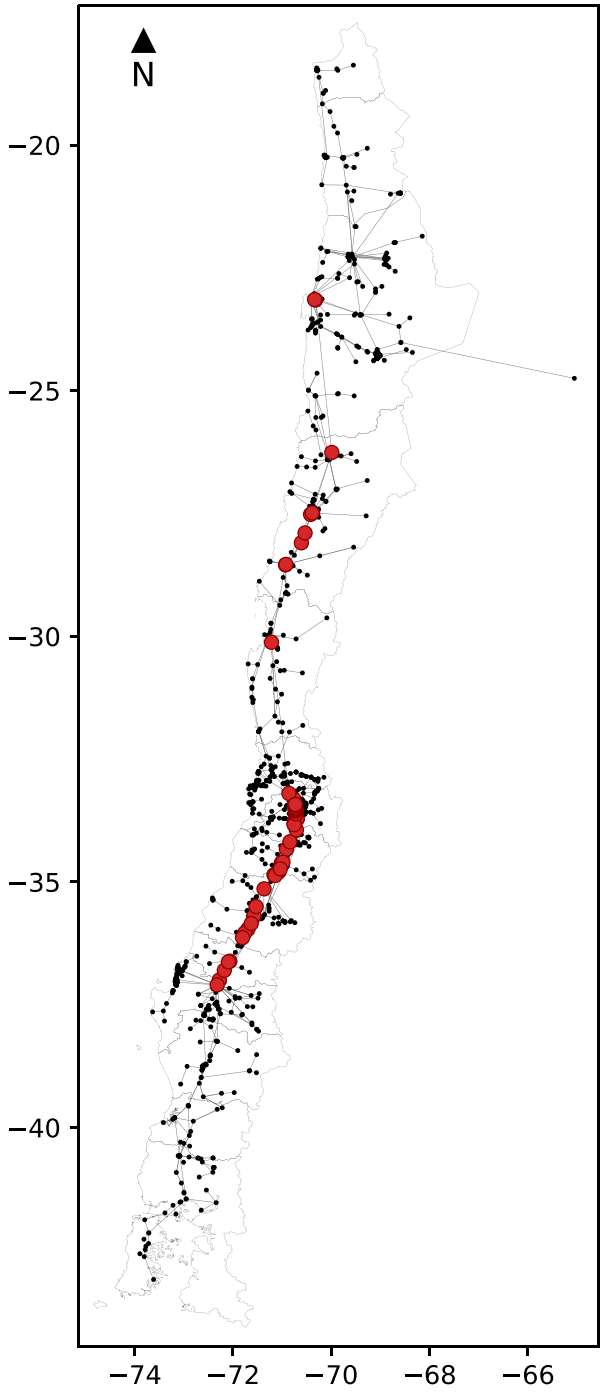

Fig. 13. Geographical distribution of the 52 substations with betweenness centrality higher than 0.3.

load nodes through the Power Transfer Distribution Factor (PTDF); and (iii) line power flow limits [73,76]. Electrical betweenness of substation n, $C_B^{ext}(n)$, is defined as half of the sum of the power flowing through the lines passing through node n [73,76]:

$$C_B^{ext}(n) = \frac{1}{2}\left(\sum_{m\in\mathcal{N}^G}\sum_{h\in\mathcal{N}^D} f^c_{m,h} \sum_{l_{ij}\in\mathscr{L}(n)} \left|\rho^{mh}_{l_{ij}}\right|\right) \tag{12}$$

where $\mathscr{L}(n)$ is the set of lines passing through node n; $\rho^{mh}_{l_{ij}}$ with $l_{ij} \in \mathscr{L}(n)$, is the PTDF of all lines passing through node n when power is injected at node m, and demand is at node h; and $f^c_{m,h}$ is the power transmission capacity from nodes m to h and it is computed from the line power flow limit and the PTDF [73].

3.2. Topological measures of the Chilean EPN case study

The histograms, minimum, maximum, mean and median values of the TMs just defined were computed for the Chilean EPN (Fig. 11); TMs were computed for the EPN considering all components without damage. A close-up of the tails of the histograms is also given.

Except for the closeness centrality, all parameters decay exponentially in value. For closeness, the distribution shows that most of the substations are on average closer to the generation units (larger closeness). This is the case because of the well distributed power generation units and the long and narrow shape of the country. Thus, substations with the lowest values of closeness are located in the northernmost and southernmost regions, which are farther on average from all generation units. This is illustrated in Fig. 12, where the closeness centrality for all load substations is reported. Load substations are grouped by region and from north (left) to south (right). Regions in the north of Chile are farther on average from generation units than regions in the south. This is due to the fact that the highest number of generation units is located in the Biobío region (south), with around 16% of the total installed power generation units. Although the region with the highest installed power generation capacity is the Antofagasta region (north) with more than 26% of the total installed power generation capacity, more generation units are present in the Biobío region. The well distributed nature of power generation units can also be noticed in the histogram showing the minimum distance to a source (Fig. 11, plot (1,3)). Indeed, most load substations are very close to at least one generation unit: on average the minimum distance is 18 km and the median is 9 km.

In Fig. 11, the histogram of the betweenness centrality (plot (1,2)) shows two clear sets of nodes in the EPN. The first one is characterized by betweenness centrality below 0.17 and the second one, in the tail, with values above 0.3. Betweenness centrality for the former set is smaller than for the latter. The latter represents nodes of the network that belong to a set of substations that are part of substantially more critical paths. The total number of critical substations is 52 and their geographical distribution is shown in Fig. 13. As it should be expected, these nodes are along the backbone of the EPN. Nodes in the center are characterized by higher betweenness than nodes in the periphery of the EPN. A core-periphery structure characterizes the Chilean EPN with nodes in the core highly interconnected among each other and peripheral nodes weakly connected to other peripheral nodes [77].

Each of the topological parameters of Fig. 11 summarizes a lot of information on the structure of the network. A more informative interpretation of these values would require comparison with those of other EPNs. Despite this shortcoming, the degree seems to have the best correlation with risk metrics. An exponential distribution fits well the degree in plot (1,1) of Fig. 11, with 0.76 as a parameter, which is slightly higher but in agreement with the exponential parameters associated with the degree distribution of the North American power grid [44] and the Italian high-voltage (380 kV) electrical transmission network [50], which equal to 0.5 and 0.55, respectively. Therefore, the Chilean EPN can be classified as a single-scale network characterized by a degree with a fast decaying tail [78]. The separation of some nodes with larger degrees is characteristic of the so-called "hubs" in the network. The two largest hubs correspond to "Charrua", in the Biobío region, and "Cardones", in the Atacama region with degrees 28 and 18, respectively, implying a large connectivity relative to the median value of 2.

Fig. 14 presents scatter plots between these TMs for the network. It is apparent that the highest correlation coefficients occur between entropy degree and electrical betweenness ($R = 0.870$), entropy degree and degree ($R = 0.720$), and degree and electrical betweenness ($R = 0.622$).

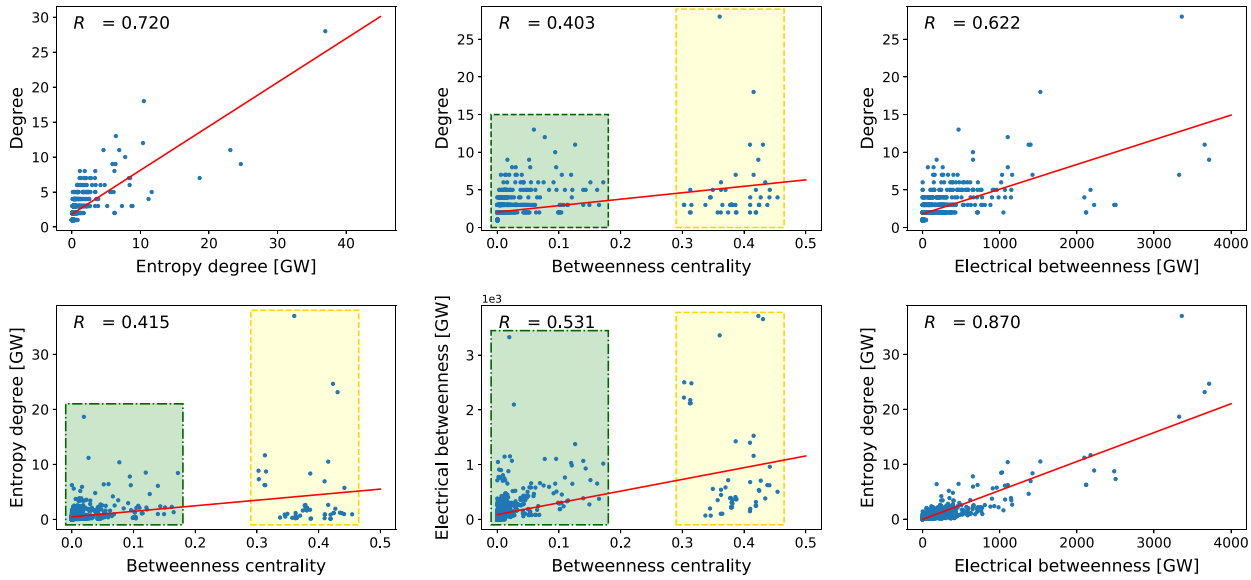

Fig. 14. Relationships between four TMs for all substations; Pearson correlation coefficients and linear regression are also reported.

Table 1
Pearson coefficients and associated 95% confidence intervals (in brackets) between the TMs and the risk analysis results. The "*" symbol denotes intervals that contain the zero value.

	EAL_{ENS}	$\overline{EAL_{ENS}}$	EAL_{hr}
Degree	0.188 [0.094, 0.279]	−0.250 [−0.338, −0.158]	−0.238 [−0.326, −0.145]
Betweenness	0.065 [−0.031, 0.160]*	−0.131 [−0.224, −0.035]	−0.124 [−0.217, −0.029]
Entropy degree	0.210 [0.117, 0.300]	−0.083 [−0.178, 0.012]*	−0.086 [−0.181, 0.010]*
Electrical betweenness	0.122 [0.027, 0.216]	−0.166 [−0.258, −0.071]	−0.16 [−0.252, −0.065]
Closeness	0.005 [−0.091, 0.101]*	0.090 [−0.006, 0.184]*	0.186 [0.092, 0.277]
Minimum distance	−0.023 [−0.119, 0.073]*	0.195 [0.101, 0.285]	−0.028 [−0.123, 0.068]*

This correlation provides an idea of consistency between network structural measures. The betweenness parameter also shows some interesting features. Plot (1,2) in Fig. 14 shows two clusters of nodes (green and yellow boxes) with similar degrees but very different betweenness. The yellow cluster presents higher betweenness values and includes 52 substations (Fig. 13). The two substations with the highest degree belong to this cluster in agreement with their higher number of neighbors and a higher probability that the shortest path passes through this node. However, other critical substations identified by betweenness centrality also have a low degree equal to 2, proving that for betweenness the central or peripheral location of a node is more relevant than the number of connections. A very similar observation is obtained by looking at plots (2,1) and (2,2), which correlate betweenness with entropy degree and electrical betweenness, respectively. Substations with the highest values of electrical betweenness and entropy degree are also identified as critical by the betweenness centrality. However, there are a few exceptions, given by substations "Ancoa" and "Seccionadora Lo Aguirre", which are ranked as critical by the two extended TMs, but they do not lie on the yellow rectangular cluster of nodes with highest values of betweenness centrality.

3.3. Seismic risk versus topological measures

Previous research has shown that coupling of the grid network can be represented by the algebraic equation [79] $YU = I$, where U and I represent the bus voltage and injected current vectors; and Y is the network admittance matrix, which depends not only on the topology (structure) of the network but also on its electrical parameters. This equation implies that the criticality of electrical components identified by centrality measures are coupled with the electrical quantities. This Section evaluates such relationships by relating the earthquake affected power flow model results with those of the network structure.

A summary of the correlation between network TMs and network performance is presented first. In Table 1, Pearson correlation coefficients between TMs and risk analysis results, EAL_{ENS}, $\overline{EAL_{ENS}}$, and EAL_{hr}, at the component level are shown together with the corresponding 95% confidence intervals. TMs consider only load substations since EAL values are only associated with this set of nodes. It is observed that most correlation coefficients are close to zero, with the highest absolute value being 0.25. Therefore, there is no clear linear correlation between TMs and EAL measures; however, a trend appears by looking at the sign of the coefficients. Negative signs, say, between the degree and the $\overline{EAL_{ENS}}$, or the degree and the EAL_{hr}, imply that the higher the degree, the lower the $\overline{EAL_{ENS}}$, and the lower the EAL_{hr}, as expected. Instead, positive signs between the minimum distance to a generation unit and $\overline{EAL_{ENS}}$, imply that the longest the minimum distance to a generation node, the larger $\overline{EAL_{ENS}}$, also as expected. Positive correlations for EAL_{ENS} are due to its strong positive correlation with energy demand. Indeed, the higher the energy demand, the higher the EAL_{ENS} (Fig. 10). Regarding closeness centrality, positive correlations, specifically the one with EAL_{hr} show that the closer a substation to all generation units, the higher the EALs. This is somewhat unexpected, but it suggests that for the Chilean EPN, adding new generation units may not be the most efficient solution to decrease *EALs*. The 95% confidence intervals confirm the lack of linear correlation between the corresponding relationships.

Scatter plots between the six TMs and *EALs* are presented in Fig. 15. Pearson correlation coefficients and the median relationship for each parameter and EAL relationship (solid lines) are presented. The clearest trends are those with the node degree, and the largest the degree, the lower the $\overline{EAL_{ENS}}$ and EAL_{hr}. Thus, a component with fewer connections tends to have larger *EALs*. Again, betweenness plots show the presence of the same hubs in the network with the 52 substations illustrated in Fig. 13. In all plots, the variability observed for a given TM is significant and hence, it conveys the idea that the structure of the EPN and

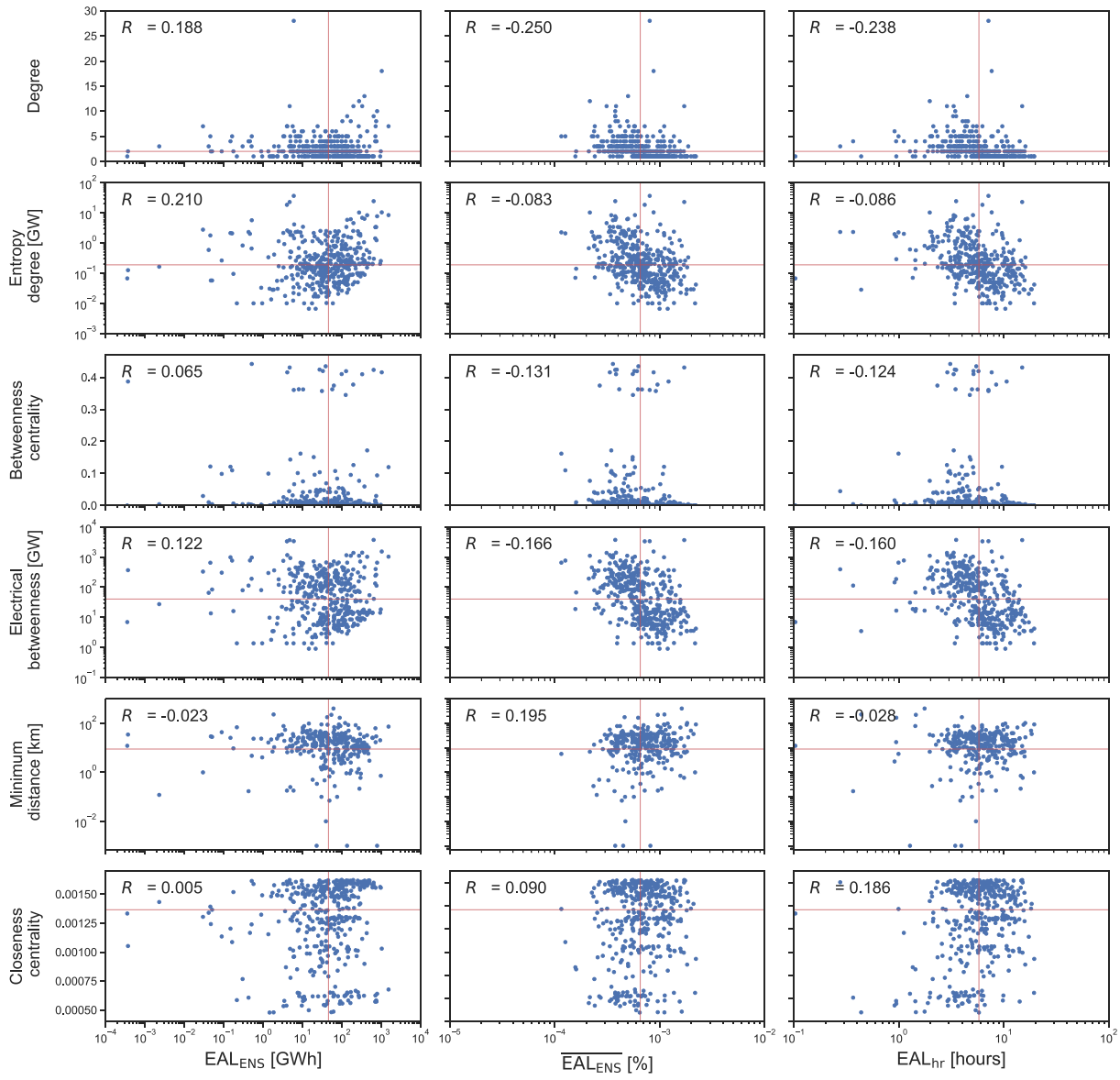

Fig. 15. Relationships between TMs and EAL values; median values (solid lines) and Pearson correlation coefficients (R) are also reported.

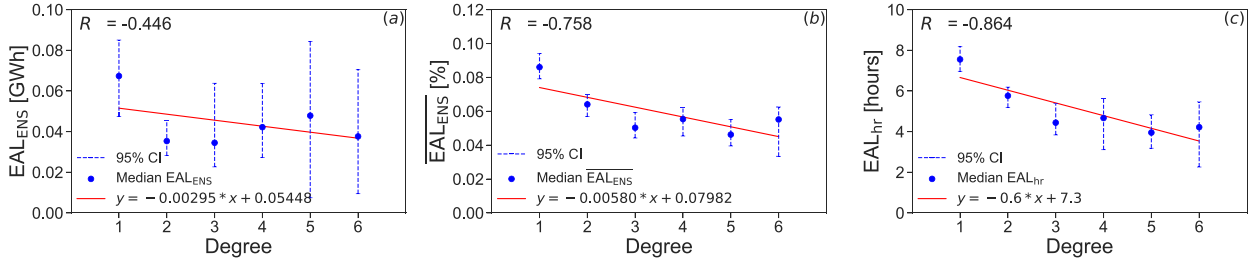

Fig. 16. Pearson correlation coefficients R, and linear regressions between the degree measure for values from 1 to 6 and the median of: (a) EAL_{ENS}, (b) $\overline{EAL_{ENS}}$, and (c) EAL_{hr}. The 95% confidence intervals on the median EALs are also reported.

centrality measures are not strongly correlated with the losses in network performance. This statement has several interpretations and some relevant exceptions, such as the negative correlation between the $\overline{EAL_{ENS}}$ and the EAL_{hr} with the node degree and electrical betweenness. The shape of the scatter plots involving closeness centrality (last row of Fig. 15) may also suggest that generation units are well distributed and *EALs* are not strongly correlated with this measure. Trends in correlation are not obvious from these plots, which may imply a well distributed risk in the network.

Given the larger correlation observed with the degree parameter, an

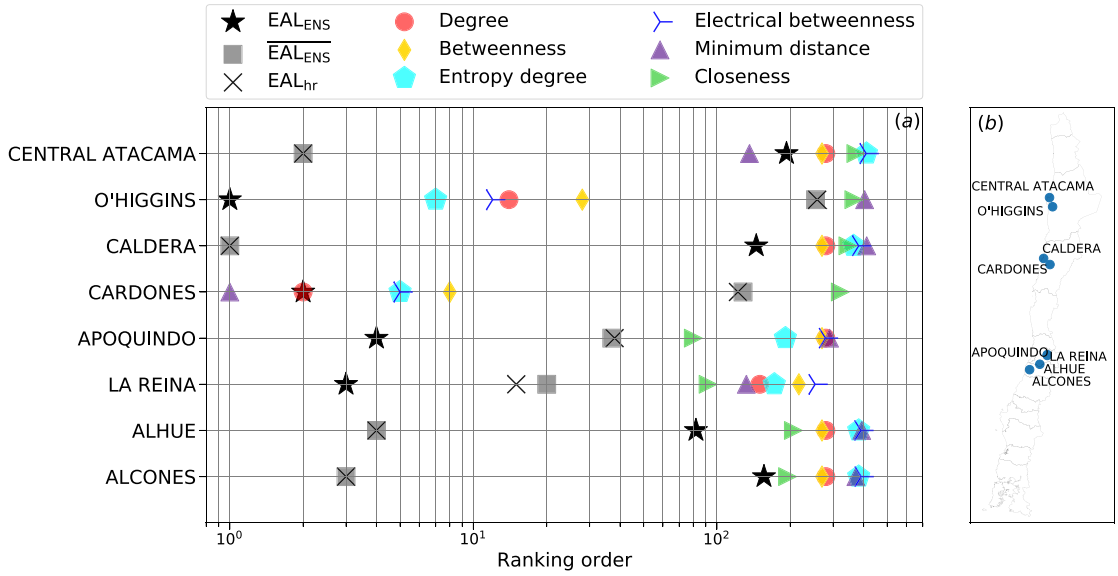

Fig. 17. Comparison of TM and EAL rankings: a) ranking order of 8 relevant load substations of the EPN—markers indicate EALs and TMs; and (b) geographical distributions of these load substations.

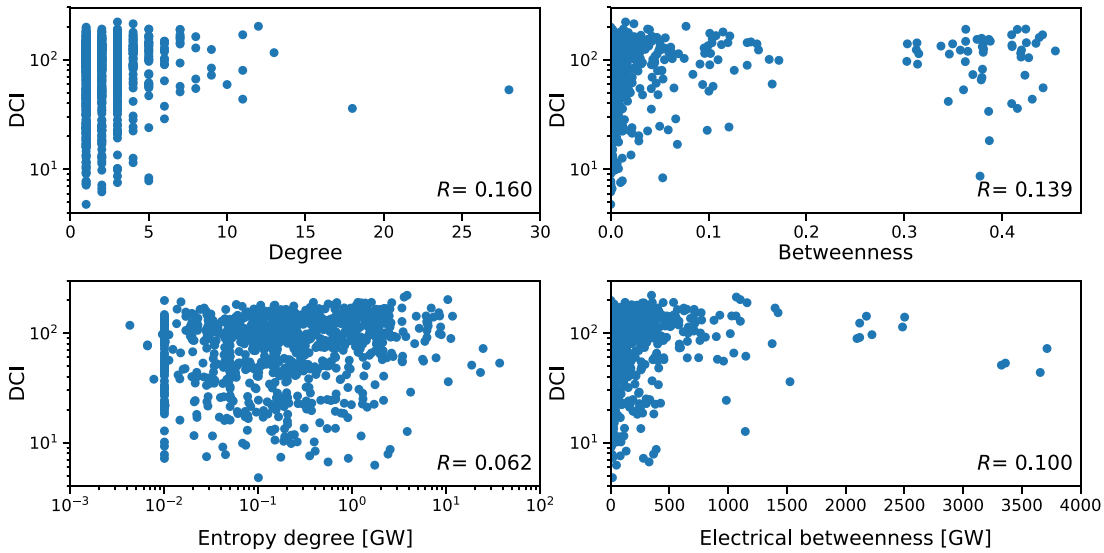

Fig. 18. Relationship between DCI and TMs considering all substations.

additional regression analysis was performed between the degree and the median values of the risk results. This was possible since degree values are discrete, as opposed to other TMs. Degrees higher than 6 have been neglected since they are associated with a small number of load substations (< 9) and the medians of the *EAL* values are not accurate. Fig. 16 presents the median values of the EAL_{ENS}, $\overline{EAL_{ENS}}$ and EAL_{hr} as a function of degree. Pearson correlation coefficients and linear regressions are also presented with their corresponding 95% confidence intervals. The correlation coefficients considering the median *EAL* values are considerably higher than reported earlier (Table 1). Results show that the higher the degree, the lower the median for the *EALs*. Then, from all the centrality parameters, the degree seems to be an important indicator to improve the EPN performance under severe earthquake actions.

Shown in Fig. 17 are the TM rankings of 8 relevant load substations of the EPN according to their *EALs*. Four substations are the most critical with respect to EAL_{ENS} and other 4 substations are the most important with respect to $\overline{EAL_{ENS}}$ and EAL_{hr}. For each substation, the marker represents the ranking order of a specific *EAL* and TM; higher values of all TMs are ranked first (in descending order), except for the minimum distance to a source which is ranked in ascending order. The plot on the right shows the geographical location of these substations, which belong mostly to the center/north of the country, and five are closer to the coast rather than the central valley. It is apparent that there is no strong consistency between the different rankings of the TMs and the *EALs* rankings. Indeed, with the exception for substation *O'Higgins*, which is within the first 28 critical load substations in terms of degree, betweenness, entropy degree and electrical betweenness, and substation *Cardones*, which is among the first 8 critical also in terms of the minimum distance, the other load substations do not seem to present high-ranking TMs.

Among several factors, the lack of consistency between the different rankings may be the result of the integration of the network. It implies that the *EALs* do not occur only as a result of the structural properties

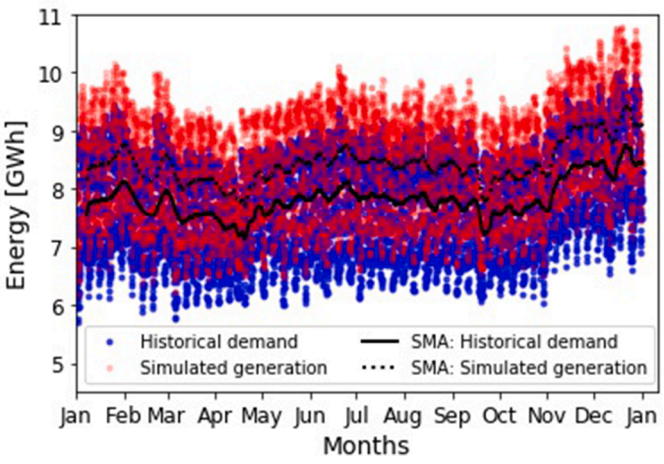

Fig. 19. Heat maps of DCI with cell size equal to 0.07°, on the left, and 0.15°, on the right, and 0.025° in the close-ups.

Table A.1
Notation used in the formulation of the DC—OPF model.

Notation	
Decision variables	**Variables**
$f_{l,n}^{in}$: power flow through line l that enters node n [MWh]	D_n: energy demand of substation n [MWh]
$f_{l,n}^{out}$: power flow through line l that leaves node n [MWh]	N_{island}: number of islands that may be generated
LS_n: load shedding (or ENS) of substation n [MWh]	P_g^{hist}: historical value of power generation of unit g [MW]
P_g: power generated by unit g in one hour [MWh]	u_g^{op}: functionality of power generation unit g
θ_n, θ_h: voltage angles of substations n and h at the end of line l	u_l^{op}: functionality of line l
Parameters	**Sets**
c_g^{gen}: cost of power generation [US$/MWh] of unit g	$\mathscr{G}$: set of power generation units
c_n^{LS}: service interruption cost [US$/MWh] of substation n	$\mathscr{G}(n)$ set of power generation units connected to node n
f_l^{max}: maximum capacity of line l [MW]	$\mathscr{G}^T$: set of thermal power plants
P_g^{max}: nominal power generation capacity of unit g [MW]	$\mathscr{G}^R$: set of renewable power plants
S_0: base power, set to 100 MVA	$\mathscr{N}$: set of substations
x_l: reactance of line l [p.u.]	$\mathscr{N}(l)$: set of end nodes of line l
τ^{loss}: power loss factor	$\mathscr{L}$: set of all lines
$\theta_{n_{ref}^{isl}}$: voltage angle of the reference node(s)	$\mathscr{L}(n)$: set of lines reaching node n

(topology) of the network, but rather depends on the characteristics of the energy flow model. Indeed, given the component redundancy present in the network, it is possible that the EPN can supply the required energy demand even when some of its components are unavailable. In other words, a given network structure with damaged components may, or may not, reach the energy supply and demand equilibrium point depending on the level of energy demand, not only on the current status of the network structure.

EALs rank substations that are associated with energy demand. In order to extend this analysis to a complete ranking of substations, the Damage Consequence Index (DCI) [54] was also tested. The DCI is computed from the System Serviceability Index (SSI) that is a random variable that depends for each earthquake realization (scenario) k on the ratio between the energy supplied after the earthquake including potential damage, P_s^d, to that of the unperturbed system prior to the earthquake, P_s^o, at the system level. SSI values range from 0 to 1, where SSI = 0 and 1 denote full loss of service and full functionality, respectively. SSI is computed only for the first hour after the earthquake and ignores the recovery process, and is defined as [54]:

$$SSI_k = \frac{\sum_{n\in\mathscr{N}}\left(P_s^d\right)_n}{\sum_{n\in\mathscr{N}}\left(P_s^o\right)_n} \tag{13}$$

and hence, the DCI of component n is given by:

$$DCI_n = \frac{E[SSI] - E[SSI|L_n]}{1 - E[SSI]} \tag{14}$$

where $E[SSI]$ represents the expected value of SSI considering all earthquake realizations; and $E[SSI|L_n]$ is the conditional expected value of SSI given that substation n has been damaged by the earthquake, i.e. considering a subset of earthquake realizations for which component n was damaged. DCI reflects a percentual reduction of SSI given the damage of component n. Thus, the larger the value of the DCI for component n, the higher the component criticality.

Since DCI is computed for every substation, its relationships with the corresponding TMs are given in Fig. 18. The relationship between degree and DCI shows a positive correlation, which means that a component with higher degree has larger DCI. Such is the case because a component with a large number of connections usually leads to a larger mean impact if damaged. This is consistent with the relationship between degree and EAL_{ENS} (Fig. 15) for load substations. Note that this is not in contradiction with the relationships between the degree and the $\overline{EAL_{ENS}}$ and EAL_{hr} (Figs. 15 and 16) that showed the importance of increasing the degree to reduce the *EAL*. Indeed, these are competing effects, since a substation with a high number of connections can produce a strong impact on the system if damaged, but at the same time, if it is not damaged, still plays an important role in connecting the network to reduce the overall losses. Also, a positive correlation, though small, is observed between DCI and betweenness centrality.

Fig. 19 shows a heat map of DCI values for the country. The color in each cell is computed by the average DCI of all substations within the cell. Lighter colors represent larger DCI values, i.e. more critical components, while darker colors less critical ones. The uniformity of colors for the complete map of the country reflects that all regions have certain critical components, while a larger density of such components is clearly observed in the mining region of the north, the metropolitan regions in central Chile, and a smaller cluster in the Concepcion and Arauco area in the south. Close-ups of these regions are also presented in the Figure to improve legibility. Maps with different cell sizes are also presented to better show these three clusters in the country.

4. Conclusions

This work sought to: (i) quantify seismic risk and resilience of the Chilean EPN exposed to earthquake hazard; and (ii) investigate which parameters of the structure of the network better correlate with earthquake risk and identify critical nodes and network clusters of the Chilean EPN. Seismic risk and resilience evaluations were carried out at national, regional and component level by using the SPRA framework. MAFs of exceedance were obtained for: (i) the expected value of the annual ENS (EAL_{ENS}); (ii) the expected value of the annual ENS normalized by the annual energy demand ($\overline{EAL_{ENS}}$); and (iii) the expected annual duration, in hours, of ENS (EAL_{hr}). Furthermore, this study sought to correlate the three EAL measures with the energy demand for each load substation.

Seismic risk and resilience results at national level show that earthquake risk of the Chilean EPN is characterized by an expected annual ENS (EAL_{ENS}) near to 45 GWh, which is equivalent to approximately 6 h of blackout for the entire country at full capacity. Furthermore, the total expected number of hours with unsupplied energy (EAL_{hr}) in any substation is equal to 16.5 days. Qualitatively, these results are consistent with the impact after the 2010 Maule earthquake in Chile. At the component level, positive correlations occur between EAL_{ENS} and energy

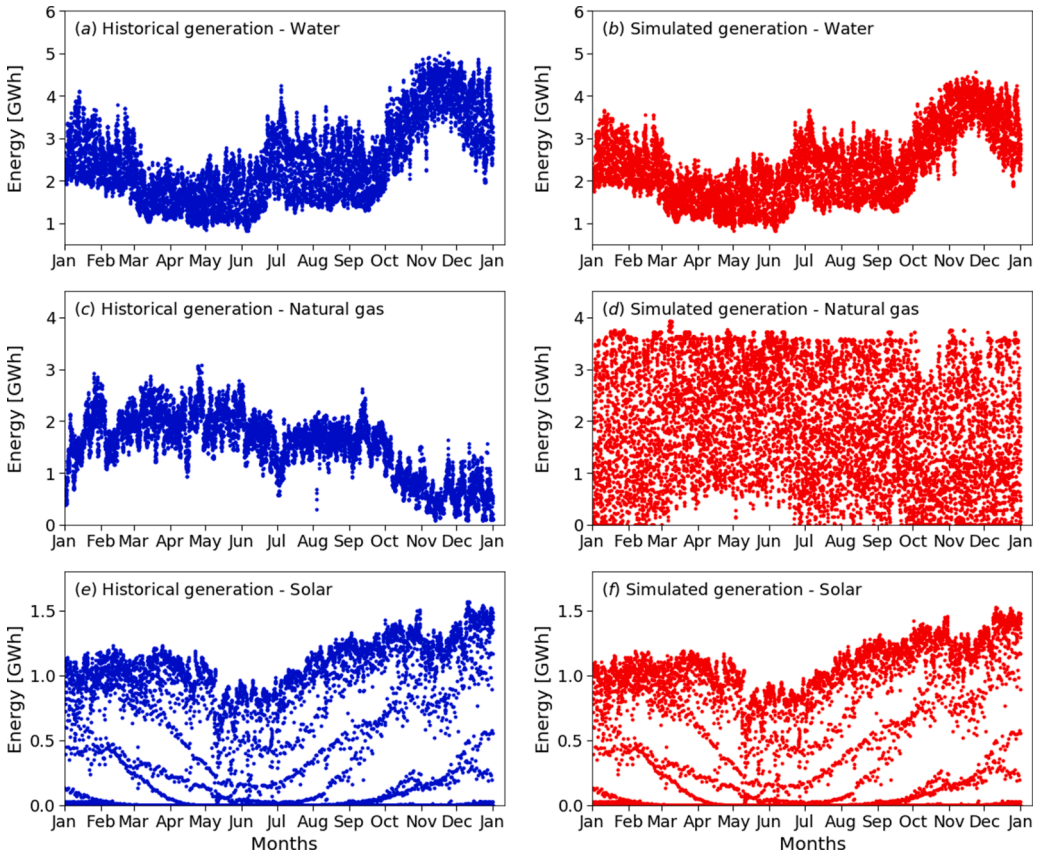

Fig. C.1. Historical hourly energy demand profile and the hourly energy generation profile obtained by simulation. Simple Moving Averages (SMAs) for a period of one week are also given.

Table C.1
Power generation aggregated for type of generation technology: comparison between historical data and simulation results.

Sources of energy generation	Historical data		Simulation results	
	GWh	%	GWh	%
Coal	28,340	38.36	25,296	34.24
Water	21,768	29.46	20,755	28.09
Natural gas	13,321	18.03	16,630	22.51
Solar	3841	5.2	3800	5.14
Wind	3490	4.72	3421	4.63
Biomass	2456	3.32	3295	4.46
Oil	614	0.83	634	0.86
Geothermal	58	0.08	58	0.08
Total power generation	73,888	100.00	73,890	100.00

demand, showing that load substations with higher demand undergo higher energy losses. Positive correlation also occurs between $\overline{EAL_{ENS}}$ and EAL_{hr}, showing that a load substation with higher percentage of ENS relative to its demand may also be affected by a longer period of operational disruption.

Topological centrality measures, degree, betweenness centrality, closeness centrality, minimum distance to a source, entropy degree and electrical betweenness were also computed and correlated with risk results at component level. In addition, DCI was obtained for all substations and used as a proxy to identify substations that if damaged, lead to larger reductions of the system's serviceability, and which geographical areas concentrate most critical components. Results suggest a well distributed risk in the Chilean EPN. It is concluded that component rankings differ depending on the EAL considered. Degree and betweenness identify the existence of hubs and structures present in the EPN. It is also shown that components identified as critical by TMs are not necessarily critical in terms of risk or DCI.

It is concluded herein that TMs provide limited insight on the criticality of the current Chilean EPN subject to earthquake hazard. This is the case because the network structure does not account for important aspects of the hazard, energy flow model, and component fragilities. Among all TMs, and within a range of values, the best (linear) correlation is obtained between the degree and median values of the EALs. Thus, increasing the degree of the EPN may reduce the median of the EAL, which is an intuitive, but important result. It is also apparent that identical network structures, and hence identical TMs, located in different seismic settings will respond very differently. Consequently, network structure is not sufficient to capture risk, since it neglects important local aspects related to the seismic hazard and component fragilities.

To the best of our knowledge, this is the first time seismic risk has been evaluated for the complete Chilean EPN with this level of detail. Moreover, the comprehensive evaluation of the correlation between several TMs and earthquake risk applied to the real EPNs is also novel. The EPN model developed can be sophisticated further by improving the detailed representation of the fragilities of the different network assets, which is a current aim of our research. Indeed, region-specific fragility functions and downtime functions, for EPN network assets, and the evaluation of the epistemic uncertainty at several stages of the seismic risk framework proposed should be evaluated in the future. Future work should also propose better metrics capable to better identify most critical network assets in order to better support decision-making in preliminary earthquake risk assessments of the EPN, avoiding the more complex risk estimations. Also, aggregated EALs used in the analyses may also conceal relevant correlations and other risk and resilience metrics should be explored. We also recommend to compare these risk results with results from other national EPN models to possibly

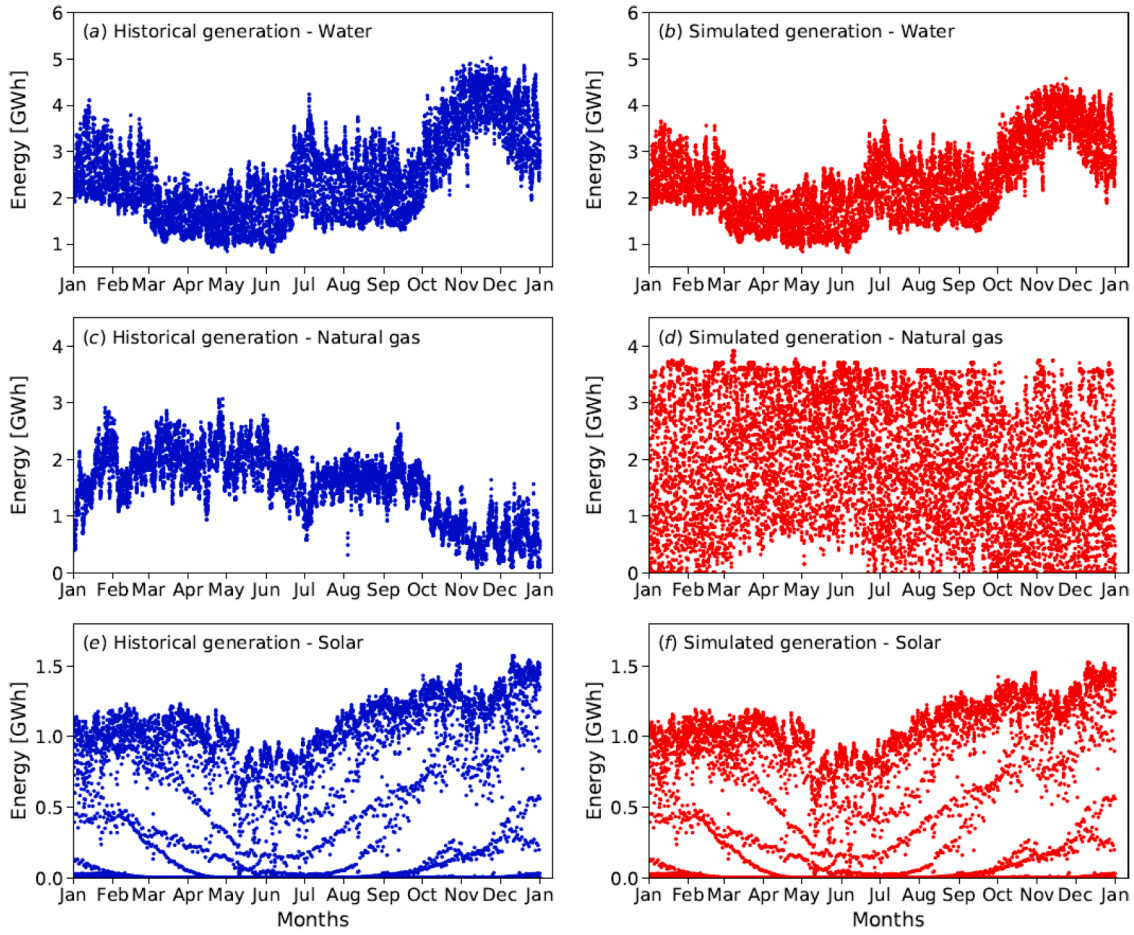

Fig. C.2. Historical (left) and simulated (right) hourly energy generation profiles from hydraulic-based power generation units (a and b); natural gas-based power generation units (c and d); and solar-based power generation units (e and f).

Table C.2
RMSE between the hourly generation profiles considering historical data and simulation results.

Sources of energy generation	RMSE [MWh]
Natural Gas	1183
Coal	515
Oil	236
Water	176
Biomass	128
Wind	17
Solar	12
Geothermal	0

generalize some of the observations presented herein.

Finally, please note that risk and resilience values are strongly affected by the seismic capacity of network components, which have been considered homogeneous for the entire country. Indeed, fragility functions of substations and generation units are only differentiated by their voltage level and size, respectively, but no distinction was made based on geographical location, which seems to be a reasonable assumption given the enforcement of uniform seismic codes in their design and construction practice.

CRediT authorship contribution statement

E. Ferrario: Conceptualization, Methodology, Software, Data curation, Writing – original draft, Writing – review & editing, Visualization, Funding acquisition. **A. Poulos:** Methodology, Software, Writing – original draft, Writing – review & editing. **S. Castro:** Software, Data curation, Visualization. **J.C. de la Llera:** Conceptualization, Methodology, Resources, Writing – original draft, Writing – review & editing, Supervision, Funding acquisition. **A. Lorca:** Methodology, Data curation, Writing – review & editing, Funding acquisition.

Declaration of Competing Interest

The authors declare that they have no known competing financial interests or personal relationships that could have appeared to influence the work reported in this paper.

Acknowledgement

This study has been sponsored by the Chilean Research and Development Agency (ANID) under Fondecyt grants #3180464, #1170836, and #11170423, and by the Chilean Research Center for Integrated Disaster Risk Management ANID/FONDAP/15110017 (CIGIDEN). The authors also wish to thank engineers Alfredo Oneto and Camilo Magnere for their support in the process of data collection and the Chilean EPN model construction.

Appendix A. Notation of the DC—OPF model

In Table A.1, the notation used in the formulation of the DC—OPF model of Section 2.2 is reported.

Appendix B. Chilean EPN

In this Appendix, a synthesis of the data collection process of power generation units, substations, transmission lines and loads of the Chilean EPN is reported together with the associated limitations. Further details are presented elsewhere [60].

Data related to power generation was collected at the unit level since large power plants can be composed of several power generation units, which can operate with different types of fuel and costs. In total, 500 power generation units were identified in the country (2017) with an installed total power generation capacity of 21,900 MW, characterized by a matrix of primary energy sources: coal (18.6%), oil (15.6%), natural gas (18.5%), biomass (1.9%), water (30.6%), wind (5.1%), solar (9.5%), and geothermal energy (0.2%). Geographical coordinates of power plants are provided elsewhere [65,66]; electrical information, such as installed power generation capacity and connection substations, which are used by power plants to inject power into the grid, were retrieved from the Coordinator [65], whereas individual hourly energy generation profiles during 2017 and type of generation technology (i.e. fuel used) for each power generation unit, were taken from *Energía Abierta* [67], since historical power generation profiles were given only at a monthly resolution level in the database of the Coordinator. From the collected data, the total energy generated during 2017 equals 73,888 GWh, which is consistent with the value reported in the Coordinator's annual report of the EPN where the total energy generated is 74,222 GWh [80].

Information about the cost of power generation for each unit is required in the model. This cost is given by the sum of fixed and variable generation costs; however, since unit commitment has not been carried out, fixed generation costs were neglected in the analysis, and variable generation costs were calculated as indicated elsewhere [81]:

$$c_g^{gen} = \left(c_g^{var\_f} + c_g^{var\_nf}\right) \tag{B.1}$$

where c_g^{gen} is the variable cost of generation of unit g and it is given in [US$/MWh], $c_g^{var\_f}$ and $c_g^{var\_nf}$ are the variable costs in (US$/MWh), associated with the fuel and with other materials and processes, respectively.

A total of 994 substations have been identified for the year 2017; they include tap-offs that are small substations that allow simple connections from an electric line for energy withdrawal or power supply. Data collected for substations are geographical coordinates, voltage levels, and starting operation date. Four databases have been considered in this task since each of them was partially complete; as a result, an integrated unique and consistent database was built. The list of 994 substations has been determined considering the following data sources: (i) a substation database containing geographical coordinates and other technical information of most Chilean substations [65]; (ii) a load database providing the hourly load profile of substations [82]; (iii) a transmission line database illustrating the connections among substations [65]; and (iv) a power plant database showing the corresponding substations of connections [65]. Voltage levels of substations are detailed in the first database; however, since it has missing information, all substation voltage levels were obtained from the voltage levels of the connected lines. Starting operation date was required in the model to neglect substations that started operation after 2017. Finally, substation owners have also been identified, since different substations may have identical names, and hence the owner specifies uniquely these substations.

The total 994 substations were connected by 1195 transmission lines. Each transmission line specifies substation names at both ends, their length, capacity, voltage, and reactance [65]; however, information was missing for some lines and a laborious process of identification of missing lines and their associated technical characteristics was carried out by analyzing a georeferenced map of the EPN components, and the electrical unilinear diagram [65]. In this diagram, technical information, such as line length, voltage, and capacity is reported. Capacity values are provided at different temperature conditions, which for this work uses 20 °C under the sun. Reactance values are given in Ohms, and they were transformed in per unit (p.u.) by dividing values by the line impedance.

Substations are associated with loads that represent the total amount of energy demanded by consumers. Energy consumption is considered as a good proxy of the energy demand. Data of the hourly energy consumption for the year 2017 were retrieved from the Coordinator databases [82,83]. From the collected data, the peak in power reached 10 GW, and the total energy demand was 68,526 GWh. These values are sufficiently close to the ones informed by Coordinator's annual report on the EPN performance, which are 10.4 GW and 67,396 GWh for the peak in power and total energy demand in 2017, respectively [80].

The data collection process was extensive and laborious. The main difficulties encountered were due to disperse data in many different sources, incomplete databases and lack of data, inconsistent databases, errors in data, and preprocessing of some data. Some assumptions were imposed because of missing data of geographical coordinates and technical (electrical) characteristics of components, and inconsistencies between substation names in different databases that made critical the identification of transmission lines. Approximations were also taken from the literature in case of not available information, such as the data related to the cost of power generation of each unit.

Appendix C. Chilean EPN model validation

In this Appendix, the validation of the Chilean EPN model is illustrated, with respect to the two conditions imposed on the model, i.e. (i) to satisfy the supply of historical energy demand; and (ii) to approximately reproduce the normal operation of the actual system, despite the inaccuracies in data and assumptions made. To verify these objectives, the DC—OPF model presented earlier was simulated every hour for a time window of one year, which amounts to 8760 h, in normal condition, i.e. without the occurrence of earthquakes. The model considered as input that provided by the collected historical data for the year 2017 and its output was the hourly energy generated from each power generation unit.

Under normal conditions, power generation units are assumed to be always available to generate energy, except for those based on coal and renewable energy sources. Thermal power generation units using coal require a long (cold) startup time (up to 10 h) to enter into operation, while other units can switch on in minutes, or at most, half hour [84], which is shorter than the time step considered in this work. Therefore, given that unit commitment is not carried out, power generation units based on coal are also considered available on the basis of the historical energy generation profile. For the power generation units based on renewable energy sources, it is assumed that the maximum energy they can generate in a given hour is

equal to the energy historically produced in the same hour of the reference year (P_g^{hist} in Eq. (5)), due to their intermittent and variable nature. Other assumptions involve the system's topology and power generation costs. A fixed network structure over the entire reference year was considered, thus neglecting commercial operation dates of new components and planned maintenance activities. Furthermore, approximate power generation costs taken from available literature were employed.

To verify that the built model does not cause ENS in normal condition, a comparison between the historical hourly energy demand profile and the simulated hourly energy generation profile was carried out, as illustrated in Fig. C.1; the Simple Moving Average (SMA) for a period of one week is also reported in the Figure. Both profiles show similar behavior, but the energy generation profile seems to be shifted up, providing higher values; this is due to power transmission losses accounted for by the factor τ^{loss} in Eq. (3). This result confirms that ENS does not occur in the simulation of the built EPN in normal operation condition, so the built model is capable to fully supply the historical energy demand in normal operation condition (condition (i) above). This is critical to ensure that, for an eventual earthquake scenario, the consequences on the EPN performance may only be attributed to the disruptive event.

To verify that the built model can approximately reproduce the operation of the actual Chilean EPN in normal condition (condition (ii) above), the comparison between historical data and simulation results have been carried out with respect to the total (yearly) energy generated for each type of generation technology, as illustrated in Table C.1, where values are reported in descending order. Notice that the ranking of sources used for energy generation is the same for historical data and simulation results, and that the percentage values are quite similar.

A comparison between historical and simulated hourly energy generation profiles by type of generation technology is presented in Fig. C.2. Strong similarities are found between the energy generation profiles related to renewable energy sources, but some differences appear between energy generation profiles for thermal energy sources. For illustration purposes, the (historical and simulated) energy generation profiles associated with water, natural gas, and solar sources are presented in the Figure. Table C.2 presents the Root Mean Square Error (RMSE) between the historical and simulated energy generation profiles by technology type, in descending order. It is apparent that the model predicts well the generation of water and solar power, but less accurately that of natural gas. The same conclusion is observed by looking at the results of Table C.2.

Similarities and differences between historical and simulated energy generation profiles for the type of generation technology can be explained by the assumptions made in the simulation of the EPN in normal condition. In particular, power generation units based on renewable energy sources can generate in a given hour of the year a peak value equal to the historical energy generation; in addition, they have the lowest power generation costs. Therefore, the optimization problem prioritizes (maximizes) the energy generation from these sources, producing very similar energy profiles. Instead, thermal power generation units, except those based on coal that follow the historical energy generation, are not bounded by historical data. Also, they are always available and not constrained by ramp capacity and power reserves that are considered in the real EPN operation. Therefore, multiple solutions can be generated by the DC—OPF and each solution in a given hour is independent from the one of the previous hour, producing a cloud of points rather than a profile as illustrated in Fig. C.2(d). Finally, note that the DC—OPF model adopted in this work minimizes the costs of generation and the ENS neglecting the electricity market where different actors with different objectives can influence the energy generation and dispatch. Furthermore, safety criteria are not included, and hence, the power flow through lines is constrained only by line capacities.

Although all these assumptions alter the power generation, the built model provides a good representation of the real Chilean EPN system. In the future, improvement in the model will be carried out by collecting more precise data and accounting for some neglected aspects, such as that of unit commitment and safety criteria.

References

[1] Southwell P. Disaster recovery within a CIGRE strategic framework: network resilience, trends and areas of future work. In: SC C1 CIGRE Technical Committee; 2014.

[2] Tang AK, Eidinger JM. Chile earthquake of 2010: lifeline performance. American Society of Civil Engineers; 2013. https://doi.org/10.1061/9780784412824.

[3] Tang AK. Chapter 4: electric power systems. Tohoku, Japan, Earthquake and Tsunami of 2011. 2017. p. 225–335. https://doi.org/10.1061/9780784479834.ch04.

[4] Karagiannis GM, Chondrogiannis S, Krausmann E, Turksezer ZI. Power grid recovery after natural hazard impact, joint research center. European Union; 2017.

[5] President's Commission on Critical Infrastructure Protection, Critical foundations: protecting America's infrastructures (1997).

[6] Araneda JC, Rudnick H, Mocarquer S, Miquel P. Lessons from the 2010 Chilean earthquake and its impact on electricity supply. In: 2010 international conference on power system technology. IEEE; 2010. p. 1–7.

[7] Takewaki I. Preliminary report of the 2011 off the Pacific coast of Tōhoku Earthquake. J Zhejiang Univ-Sci A 2011;12(5):327–34.

[8] Abedi A, Gaudard L, Romero F. Review of major approaches to analyze vulnerability in power system. Reliab Eng Syst Saf 2019;183:153–72.

[9] Lee S, Choi M, Lee HS, Park M. Bayesian network-based seismic damage estimation for power and potable water supply systems. Reliab Eng Syst Saf 2020;197.

[10] Kröger W, Zio E. Vulnerable systems. Springer; 2011.

[11] Dueñas-Osorio L, Kwasinski A. Quantification of lifeline system interdependencies after the 27 February 2010 Mw 8.8 Offshore Maule, Chile, Earthquake. Earthq Spectra 2012;28:581–603.

[12] De Iuliis M, Kammouh O, Cimellaro GP, Tesfamariam S. Quantifying restoration time of power and telecommunication lifelines after earthquakes using Bayesian belief network model. Reliab Eng Syst Saf 2021;208.

[13] Guidotti R, Chmielewski H, Unnikrishnan V, Gardoni P, McAllister T, van de Lindt J. Modeling the resilience of critical infrastructure: the role of network dependencies. Sustain Resil Infrastruct 2016;1(3–4):153–68.

[14] Li B, Barker K, Sansavini G. Measuring community and multi-industry impacts of cascading failures in power systems. IEEE Syst J 2018;12(4):3585–96.

[15] Zio E. Challenges in the vulnerability and risk analysis of critical infrastructures. Reliab Eng Syst Saf 2016;152:137–50.

[16] Society for Risk Analysis Glossary (2018). https://www.sra.org/wp-content/uploads/2020/04/SRA-Glossary-FINAL.pdf.

[17] Wang J, Zuo W, Rhode-Barbarigos L, Lu X, Wang J, Lin Y. Literature review on modeling and simulation of energy infrastructures from a resilience perspective. Reliab Eng Syst Saf 2019;183:360–73.

[18] Cavalieri F, Franchin P, Buriticá Cortés JA, Tesfamariam S. Models for seismic vulnerability analysis of power networks: comparative assessment. Comput-Aided Civ Infrastruct Eng 2014;29(8):590–607.

[19] Shinozuka M, Dong X, Chen T, Jin X. Seismic performance of electric transmission network under component failures. Earthq Eng Struct Dyn 2007;36(2):227–44.

[20] Zareei SA, Hosseini M, Ghafory-Ashtiany M. Evaluation of power substation equipment seismic vulnerability by multivariate fragility analysis: a case study on a 420 kV circuit breaker. Soil Dyn Earthq Eng 2017;92:79–94.

[21] Wen B, Moustafa MA, Junwu D. Seismic fragilities of high-voltage substation disconnect switches. Earthq Spectra 2019;35(4):1559–82.

[22] Poljansek K, Bono F, Gutiérrez E. Seismic risk assessment of interdependent critical infrastructure systems: the case of European gas and electricity networks. Earthq Eng Struct Dyn 2012;41(1):61–79.

[23] Nozhati S, Sarkale Y, Chong EKP, Ellingwood BR. Optimal stochastic dynamic scheduling for managing community recovery from natural hazards. Reliab Eng Syst Saf 2020;193.

[24] Almoghathawi Y, González AD, Barker K. Exploring recovery strategies for optimal interdependent infrastructure network resilience. Netw Spat Econ 2021;21:229–60. https://doi.org/10.1007/s11067-020-09515-4.

[25] Buriticá Cortés JA, Sánchez-Silva M, Tesfamariam S. A hierarchy-based approach to seismic vulnerability assessment of bulk power systems. Struct Infrastruct Eng 2015;11(10):1352–68.

[26] Espinoza S, Poulos A, Rudnick H, de la Llera JC, Panteli M, Mancarella P. Risk and resilience assessment with component criticality ranking of electric power systems subject to earthquakes. IEEE Syst J 2020;14(2):2837–48.

[27] Lee S, Hwang S, Park M, Lee HS. Damage propagation from component level to system level in the electricity sector. J Infrastruct Syst 2018;24(3).

[28] Oboudi MH, Mohammadi M, Trakas DN, Hatziargyriou ND. A systematic method for power system hardening to increase resilience against earthquakes. IEEE Syst J 2020:1–10.

[29] Nazemi M, Dehghanian P. Seismic-resilient bulk power grids: hazard characterization, modeling, and mitigation. IEEE Trans Eng Manage 2020;67(3):614–30.

[30] Ouyang M, Liu C, Xu M. Value of resilience-based solutions on critical infrastructure protection: comparing with robustness-based solutions. Reliab Eng Syst Saf 2019;190.
[31] Lagos T, Moreno R, Espinosa AN, Panteli M, Sacaan R, Ordonez F, Rudnick H, Mancarella P. Identifying optimal portfolios of resilient network investments against natural hazards, with applications to earthquakes. IEEE Trans Power Syst 2020;35(2):1411–21.
[32] Moreno R, Panteli M, Mancarella P, Rudnick H, Lagos T, Navarro A, Ordonez F, Araneda JC. From reliability to resilience. IEEE Power Energ Mag 2020;18(4).
[33] Venkateswaran VB, Saini DK, Sharma M. Techno-economic hardening strategies to enhance distribution system resilience against earthquake. Reliab Eng Syst Saf 2021;213.
[34] Kameshwar S, Cox DT, Barbosa AR, Farokhnia K, Park H, Alam MS, van de Lindt JW. Probabilistic decision-support framework for community resilience: incorporating multi-hazards, infrastructure interdependencies, and resilience goals in a Bayesian network. Reliab Eng Syst Saf 2019;191.
[35] Sharma N, Tabandeh A, Gardoni P. Regional resilience analysis: a multiscale approach to optimize the resilience of interdependent infrastructure. Comput Aided Civ Inf 2020;35.
[36] Sharma N, Nocera F, Gardoni P. Classification and mathematical modeling of infrastructure interdependencies. Sustain Resil Infrastruct 2021;6(1–2):4–25.
[37] Li S, Stojadinovic B, Sansavini G. Resilience Evaluation Framework for Integrated Civil Infrastructure–Community Systems under Seismic Hazard. J Infrastruct Syst 2019;25(2).
[38] Li J, Dueñas-Osorio L, Chen C, Shi C. AC power flow importance measures considering multi-element failures. Reliab Eng Syst Saf 2017;160:89–97.
[39] Fang Y, Pedroni N, Zio E. Resilience-based component importance measures for critical infrastructure network systems. IEEE Trans Reliab 2016;65(2):502–12.
[40] Almoghathawi Y, Barker K. Component importance measures for interdependent infrastructure network resilience. Comput Ind Eng 2019;133:53–164.
[41] Rocchetta R, Patelli E. Assessment of power grid vulnerabilities accounting for stochastic loads and model imprecision. Electr Power Energy Syst 2018;98:219–32.
[42] Scherb A, Garrè L, Straub D. Evaluating component importance and reliability of power transmission networks subject to windstorms: methodology and application to the Nordic grid. Reliab Eng Syst Saf 2019;191.
[43] Liu Y, Wotherspoon L, Nair NKC, Blake D. Quantifying the seismic risk for electric power distribution systems. Struct Infrastruct Eng 2021;17(2):217–32.
[44] Albert R, Albert I, Nakarado GL. Structural vulnerability of the north american power grid. Phys Rev E 2004;69(2).
[45] Crucitti P, Latora V, Marchiori M. Locating critical lines in high-voltage electrical power grids. Fluct Noise Lett 2005;5(02):L201–8.
[46] Cuadra L, Salcedo-Sanz S, Del Ser J, Jiménez-Fernández S, Geem ZW. A critical review of robustness in power grids using complex networks concepts. Energies 2015;8(9):9211–65.
[47] Rosas-Casals M, Valverde S, Solé RV. Topological vulnerability of the European power grid under errors and attacks. Int J Bifurc Chaos 2007;17(07):2465–75.
[48] Crucitti P, Latora V, Marchiori M. A topological analysis of the Italian electric power grid. Physica A 2004;338(1–2):92–7.
[49] Fang Y, Zio E. Unsupervised spectral clustering for hierarchical modelling and criticality analysis of complex networks. Reliab Eng Syst Saf 2013;116:64–74.
[50] V. Rosato, L. Issacharoff, G. Gianese, S. Bologna, Influence of the topology on the power flux of the Italian high-voltage electrical network, arXiv preprint arXiv: 0909.1664 (2009).
[51] LaRocca S, Johansson J, Hassel H, Guikema S. Topological performance measures as surrogates for physical flow models for risk and vulnerability analysis for electric power systems. Risk Anal 2015;35(4).
[52] Jayaram N, Baker JW. Efficient sampling and data reduction techniques for probabilistic seismic lifeline risk assessment. Earthq Eng Struct Dyn 2010;39(10): 1109–31.
[53] Poulos A, Espinoza S, de la Llera J, Rudnick H. Seismic risk assessment of spatially distributed electric power systems. In: 16th World Conference on Earthquake Engineering, Santiago, Chile; 2017.
[54] Wang Y, Au SK, Fu Q. Seismic risk assessment and mitigation of water supply systems. Earthq Spectra 2010;26(1):257–74.
[55] Poulos A, Monsalve M, Zamora N, de la Llera JC. An updated recurrence model for Chilean subduction seismicity and statistical validation of its Poisson nature. Bull Seismol Soc Am 2019;109(1):66–74.
[56] Geersen J. Sediment-starved trenches and rough subducting plates are conducive to tsunami earthquakes. Tectonophysics 2019;762:28–44.
[57] Abrahamson N, Gregor N, Addo K. Bc hydro ground motion prediction equations for subduction earthquakes. Earthq Spectra 2016;32(1):23–44.
[58] Goda K, Atkinson GM. Intraevent spatial correlation of ground-motion parameters using SK-net data. Bull Seismol Soc Am 2010;100(6):3055–67. https://doi.org/10.1785/0120100031.
[59] Hazus-MH 2.1 technical manual. Washington, D.C.: Department of Homeland Security, Federal Emergency Management Agency, Mitigation Division; 2003.
[60] Ferrario E, Poulos A, de la Llera J, Lorca A, Onetto A, Magnere C. Representation and modeling of the Chilean electric power network for seismic resilience analysis. In: 29th European Safety and Reliability Conference (ESREL 2019); 2019.
[61] Wood AJ, Wollenberg BF, Sheblé GB. Power generation, operation, and control. John Wiley & Sons; 2013.
[62] Stephen F, Rebennack S. An introduction to optimal power flow: theory, formulation, and examples. IIE Trans. 2016;48(12):1172–97.
[63] Xia X, Elaiw AM. Optimal dynamic economic dispatch of generation: a review. Electric Power Syst. Res. 2010;80(8):975–86.
[64] Coordinador Eléctrico Nacional, Sistema eléctrico nacional, Last Accessed: march 2019 (2019). URL https://www.coordinador.cl/sistema-electrico/.
[65] Coordinador Eléctrico Nacional, Infotecnica, Last Accessed: march 2019 (2019). URL https://infotecnica.coordinador.cl/.
[66] Ministerio de Energıa, Ide energía, Last Accessed: march 2019 (2019). URL http://sig.minenergia.cl/.
[67] Comisión Nacional de Energía, Energía Abierta, Last Accessed: march 2019 (2019). URL http://energiaabierta.cl/.
[68] de la Llera JC, Rivera F, Mitrani-Reiser J, Jünemann R, Fortuño C, Ríos M, Hube M, María HS, Cienfuegos R. Data collection after the 2010 Maule earthquake in Chile. Bull Earthq Eng 2017;15(2):555–88.
[69] Nieminen J. On the centrality in a graph. Scand J Psychol 1974;15(1):332–6.
[70] Freeman LC. Centrality in social networks conceptual clarification. Soc Netw 1978; 1(3):215–39.
[71] Sabidussi G. The centrality index of a graph. Psychometrika 1966;31(4):581–603.
[72] Bompard E, Pons E, Wu D. Analysis of the structural vulnerability of the interconnected power grid of continental Europe with the integrated power system and unified power system based on extended topological approach. Int Trans Electr Energy Syst 2013;23(5):620–37.
[73] Bompard E, Luo L, Pons E. A perspective overview of topological approaches for vulnerability analysis of power transmission grids. Int J Crit Infrastruct 2015;11(1): 15–26. 7.
[74] Zio E, Sansavini G. Component criticality in failure cascade processes of network systems. Risk Anal 2011;31(8):1196–210.
[75] Zhang L, Su H, Zio E, Zhang Z, Chi L, Fan L, Zhou J, Zhang J. A data-driven approach to anomaly detection and vulnerability dynamic analysis for large-scale integrated energy systems. Energy Convers Manage 2021;234.
[76] Wu D, Ma F, Javadi M, Thulasiraman K, Bompard E, Jiang JN. A study of the impacts of flow direction and electrical constraints on vulnerability assessment of power grid using electrical betweenness measures. Physica A 2017;466:295–309.
[77] de la Llera JC, Monsalve M, Ferrario E, Allen E, Chamorro A, Castro S, Alberto Y, Arrospide F, Poulos A, Candia G, Aguirre P. Earthquake response sensitivity of complex infrastructure networks. In: 17th World Conference on Earthquake Engineering; 2020.
[78] Amaral LAN, Scala A, Barthelemy M, Stanley HE. Classes of small-world networks. Proc Natl Acad Sci 2000;97(21):11149–52.
[79] Wang J, Yan J, Xu Y, Huang K. Power flow calculation method for isolated microgrid considering the influence of harmonic power. J Eng 2017;2017(14): 2615–21.
[80] Coordinador Eléctrico Nacional, Reporte de desempeño del sistema eléctrico (2017). URL https://www.coordinador.cl/wp-content/uploads/2019/03/Reporte-Anual-2017-Art.-72-15.pdf.
[81] Comisión Nacional de Energía, Informe de costos de tecnologías de generación (2018).
[82] Coordinador Eléctrico Nacional, database provided by email by the Coordinador Eléctrico Nacional in May 2018. (2018).
[83] Coordinador Eléctrico Nacional, Explorador web de redcdec, Last Accessed: march 2019 (2018). URL https://aplicaciones-sic.coordinador.cl/redcdec/.
[84] Hentschel J, Babic U, Spliethoff H. A parametric approach for the valuation of power plant flexibility options. Energy Rep 2016;2:40–7.